NTNU – Trondheim
Norwegian University of
Science and Technology

Approximating Haze in Reflection

Approximate expressions for
two-dimensional randomly rough surfaces

Aleksander Hoel Kringstad

Master of Science in Physics and Mathematics
Submission date: June 2015
Supervisor: Ingve Simonsen, IFY

Norwegian University of Science and Technology
Department of Physics

Abstract

We give a definition of haze in reflection from two-dimensional surfaces and study this quantity for Gaussian randomly rough surfaces. A simplified model of light scattering, assuming a scalar incident plane wave, the Kirchhoff approximation and an impenetrable surface is used as a basis. Using this model, we are able to derive relatively simple approximate analytical expressions for haze. Haze is studied with and without these approximations for exponential- and Gaussian correlation functions, and we find that the approximate expressions are accurate. The model gives results comparable the to scattering of unpolarized light from a perfectly conducting surface given that we only look at the total scattered intensity and that the surface roughness is not too high.

Preface

This master's thesis is written as a conclusion to the five year integrated technology program "Applied physics and mathematics" at the Norwegian University of Science and Technology. The work was carried out at the Department of Physics at NTNU.

I would like to thank my supervisor, Ingve Simonsen, for valuable feedback while working on this thesis.

Trondheim, June 11. 2015,

Aleksander H. Kringstad

Contents

Chapter 1

Introduction

Gloss and haze are terms used in the optical industry to quantify the visual appearance of materials. Haze quantifies the fraction of light that is reflected or transmitted *away* from the specular direction if one were to shine a beam of light on to the material. Gloss on the other hand is a measure of the fraction of light that is reflected or transmitted in or around the specular direction. If a material is measured to have a high haze value it will have cloudy or blurry visual appearance. As an example, a mirror would have a low value of haze as most of the light is reflected in the specular direction. A sandblasted metal surface on the other hand would have a high value. Although mainly being a measure of the visual appearance of materials, the concept of haze has also found to be a useful quantity when studying light trapping in solar cells[9]. Gloss and haze are almost considered complimentary qualities. In fact, as defined in this thesis, gloss($\mathcal{G}$) and haze($\mathcal{H}$) satisfies the simple relation $\mathcal{G} + \mathcal{H} = 1$. For this reason, only haze will be discussed, as the results for gloss always can be easily aquired when the haze is known.

To study haze, one has to move into the field of rough surface scattering as the familiar example from electromagnetism of planar material interfaces is no longer sufficient. Lord Rayleigh was the first to consider wave scattering from a rough surface around the year 1877 when he studied light scattering from a sinusoidal surface. The study of wave scattering from rough surfaces is still an active field today with a wide range of application, though one today mostly deal with so called *randomly* rough surfaces[12]. When dealing with randomly rough surfaces, the surface is described in a statistical manner, allowing one to study scattering without knowing the particular shape of the surface in detail. This allows for results to be valid not only for one particular surface, but for a class of surfaces which, although not identical, has similar properties.

Gaussian random surfaces are the most well studied of these randomly rough surfaces and are the ones that will be considered here. If one for such a surface were to measure the height of the surface at a sufficiently high number of points and make a detailed histogram of the results, it would look like a Gaussian distribution. Surfaces obeying these kinds of statistics are practical to work with from a theoretical perspective, but can luckily also be manufactured in practice and are also found to exist in nature.

In this thesis the scattering of a scalar plane-wave by a two dimensional Gaussian random surface will be the model from which haze is studied. The Kirchhoff approximation is also assumed, neglecting multiple scattering. Analytical expressions will be given for the mean differential reflection coefficient(MDRC), the fraction of scattered power that goes into an infinitesimal angular interval around a given direction, for three common correlation functions. An approximate analytical expression for haze for two common correlation functions will be derived and tested.

Haze will be studied using these expressions and compared to results from rigorous scalar scattering simulations, which again have been found to correlate well with the scattering of EM waves off a perfect conductor, when the polarization of the scattered wave is not recorded. The results will aslo be directly compared to simulations of EM-scattering from a perfectly conducting surface.

Chapter 2

Background

The scalar scattering problem is described including the scattering geometry, an outline of the derivation of the integral equation describing the scattered field, the Kirchhoff approximation and definition of the mean differential reflection coefficient(MDRC). A section about Gaussian surfaces is then introduced, before looking at the validity of the Kirchhoff approximation for Gaussian surfaces. Sections 2.1 through 2.3 are based on the book "Designer Surfaces"[2].

2.1 Scattering geometry

The scattering system consists of an incident wave with wavevector $\boldsymbol{k}$, a randomly rough surface representing the interface between a vacuum and a hard wall, and the scattered wave as a superposition of plane waves with wavevectors $\boldsymbol{q}$. The surface is oriented so that the mean surface, which is planar, is described by $x_3 = 0$, i.e. lies in the x_1x_2-plane. Introducing the vector $\boldsymbol{x}_\parallel = (x_1, x_2, 0)$, the surface can then be described by its height deviation $x_3 = \zeta(\boldsymbol{x}_\parallel)$.

As depicted in Figure 2.1, the wave vectors are defined as:

$$\boldsymbol{k} = \frac{\omega}{c}(\sin\theta_0\cos\phi_0, \sin\theta_0\sin\phi_0, -\cos\theta_0) \tag{2.1}$$

$$\boldsymbol{q} = \frac{\omega}{c}(\sin\theta_\mathrm{s}\cos\phi_\mathrm{s}, \sin\theta_\mathrm{s}\sin\phi_\mathrm{s}, \cos\theta_\mathrm{s}). \tag{2.2}$$

Both $\boldsymbol{k}$ and $\boldsymbol{q}$ have length $\frac{\omega}{c}$. Since the x_3-component of the wave vectors always can be found when knowing the x_1 and x_2 components, the scattering problem can be described in terms of the x_1 and x_2 components of the wave vectors:

$$\boldsymbol{k}_\parallel = \frac{\omega}{c}\sin\theta_0(\cos\phi_0, \sin\phi_0, 0) \tag{2.3}$$

$$\boldsymbol{q}_\parallel = \frac{\omega}{c}\sin\theta_\mathrm{s}(\cos\phi_\mathrm{s}, \sin\phi_\mathrm{s}, 0). \tag{2.4}$$

The absolute value of the x_3-component of the wave vectors can be calculated by the function $\alpha_0()$:

$$\alpha_0(k_\parallel) = \sqrt{(\omega/c)^2 - k_\parallel^2} = \frac{\omega}{c}\cos\theta_0 \tag{2.5}$$

$$\alpha_0(q_\parallel) = \sqrt{(\omega/c)^2 - q_\parallel^2} = \frac{\omega}{c}\cos\theta_\mathrm{s}. \tag{2.6}$$

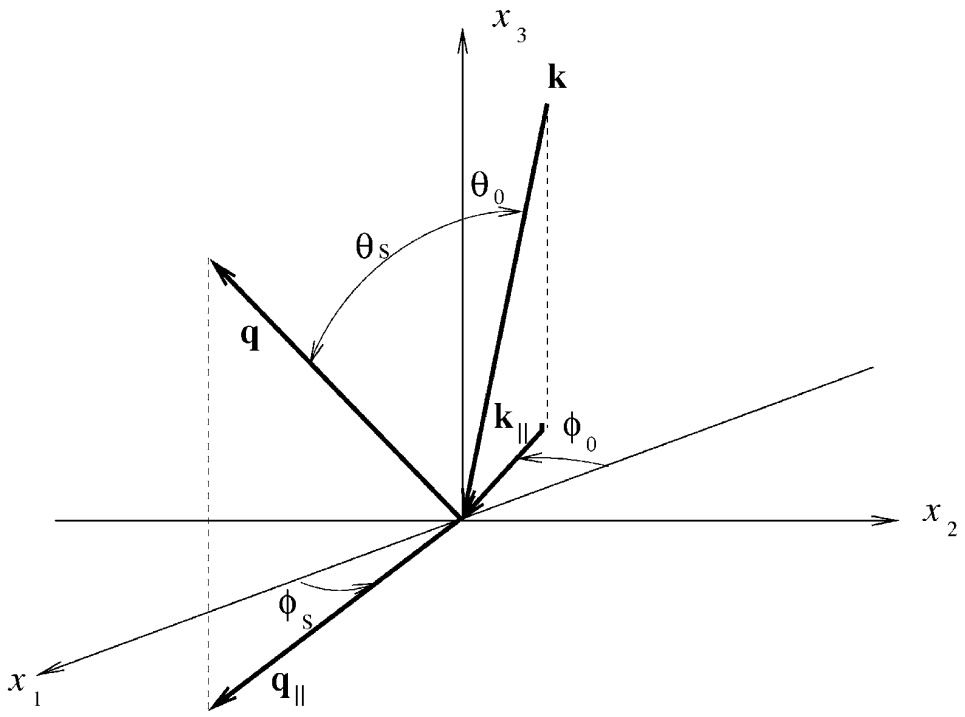

Figure 2.1: Scattering geometry

The wave vectors now can be written:

$$\boldsymbol{k}(\boldsymbol{k}_{\parallel}) = \boldsymbol{k}_{\parallel} - \alpha_0(k_{\parallel})\hat{\boldsymbol{x}}_3 \tag{2.7}$$

$$\boldsymbol{q}(\boldsymbol{q}_{\parallel}) = \boldsymbol{q}_{\parallel} + \alpha_0(q_{\parallel})\hat{\boldsymbol{x}}_3. \tag{2.8}$$

Since the $\boldsymbol{q}_{\parallel}$, $\boldsymbol{k}_{\parallel}$ will be used instead of angles, one might also want to calculate the Jacobian determinant for $\boldsymbol{q}_{\parallel}$ as given by Eq.(2.4). It relates integration over angles to integrations over q_1 and q_2, which will come in handy:

$$\mathrm{d}^2 q_{\parallel} = (\omega/c)^2 \cos\theta_s \mathrm{d}\Omega_s. \tag{2.9}$$

2.2 Wave theory

The wave in the model is scalar and satisfies the wave equation:

$$\nabla^2\Psi(\boldsymbol{x},t) - \frac{1}{c^2}\frac{\partial^2}{\partial t^2}\Psi(\boldsymbol{x},t) = 0, \tag{2.10}$$

where c is the speed of the wave. The field, $\Psi(\boldsymbol{x},t)$, is assumed to be real and monochromatic:

$$\Psi(\boldsymbol{x},t) = Re\{\psi(\boldsymbol{x}|\omega)\exp(-i\omega t)\} = \frac{1}{2}[\psi(\boldsymbol{x}|\omega)\exp(-i\omega t) + \psi^*(\boldsymbol{x}|\omega)\exp(i\omega t)]. \tag{2.11}$$

Substituing this assumed waveform into the wave equation, one sees that the complex wave amplitude, $\psi(\boldsymbol{x}|w)$, satisfies the Helmholtz equation:

$$[\nabla^2 + (\omega/c)^2]\psi(\boldsymbol{x}|\omega) = 0. \tag{2.12}$$

The wave is scattered from a rough surface defined by $x_3 = \zeta(\boldsymbol{x}_\parallel)$. The surface is assumed to be a hard wall, with no transmitted field. To describe such a surface, it is assumed that the field either is zero at the surface, the so called Dirichlet boundary condition, or that it's normal derivative at the interface is zero, the Neumann boundary condition. The Dirichlet boundary condition will be assumed here :

$$\psi(\boldsymbol{x}|\omega)|_{x_3=\zeta(\boldsymbol{x}_\parallel)} = 0. \tag{2.13}$$

The free-space scalar Green's function of the Helmholtz equation has the form:

$$g_0(\boldsymbol{x}|\boldsymbol{x}') = \frac{\exp(i(\omega/c)|\boldsymbol{x}-\boldsymbol{x}'|)}{|\boldsymbol{x}-\boldsymbol{x}'|} = \int \frac{\mathrm{d}^2k_\parallel}{(2\pi)^2}\frac{2\pi i}{\alpha_0(k_\parallel)}\exp(i\boldsymbol{k}_\parallel\cdot(\boldsymbol{x}_\parallel-\boldsymbol{x}'_\parallel)+i\alpha_0(k_\parallel)|x_3-x'_3|), \tag{2.14}$$

and is defined so that it satisfies the equation

$$[\nabla^2 + (\omega/c)^2]g_0(\boldsymbol{x}|\boldsymbol{x}') = -4\pi\delta(\boldsymbol{x}-\boldsymbol{x}'). \tag{2.15}$$

Green's second integral theorem reads:

$$\int_\Omega \mathrm{d}^3x(u\nabla^2 v - v\nabla^2 u) = \int_\Sigma \mathrm{d}S(u\frac{\partial v}{\partial \nu} - v\frac{\partial u}{\partial \nu}), \tag{2.16}$$

where Σ is the surface bounding the volume Ω and $\frac{\partial}{\partial\nu}$ is the derivative with respect to the normal to the surface Σ, pointing outward. Using Green's second integral theorem for $u(\boldsymbol{x}) = \psi(\boldsymbol{x}|\omega)$ and $v(\boldsymbol{x}) = g_0(\boldsymbol{x}|\boldsymbol{x}')$ and letting Ω be the volume bounded by the rough surface $x_3 = \zeta(\boldsymbol{x}_\parallel)$ and a hemispherical cap of infinite radius in the upper half space, in addtion to using Eqs. (2.12) and (2.15), one gets:

$$\begin{aligned}-4\pi\theta(x_3-\zeta(\boldsymbol{x}_\parallel))\psi(\boldsymbol{x}|\omega) = &-\int_S \mathrm{d}S\left[\psi(\boldsymbol{x}|\omega)\frac{\partial}{\partial n}g_0(\boldsymbol{x}|\boldsymbol{x}') - g_0(\boldsymbol{x}|\boldsymbol{x}')\frac{\partial}{\partial n}\psi(\boldsymbol{x}|\omega)\right]\\ &+\int_{S^{(+\infty)}}\mathrm{d}S\left[\psi(\boldsymbol{x}|\omega)\frac{\partial}{\partial \nu}g_0(\boldsymbol{x}|\boldsymbol{x}') - g_0(\boldsymbol{x}|\boldsymbol{x}')\frac{\partial}{\partial \nu}\psi(\boldsymbol{x}|\omega)\right].\end{aligned} \tag{2.17}$$

Here S denotes the part of Σ that coincides with the surface $x_3 = \zeta(\boldsymbol{x}_\parallel)$, while $S^{(+\infty)}$ is the hemispherical cap. Assuming the Dirichlet boundary condition, Eq. (2.17) can be rewritten :

$$\theta(x_3-\zeta(\boldsymbol{x}_\parallel))\psi(\boldsymbol{x}|\omega) = \psi(\boldsymbol{x}|\omega)_{\mathrm{inc}} - \frac{1}{4\pi}\int \mathrm{d}^2x'_\parallel[g_0(\boldsymbol{x}|\boldsymbol{x}')]_{x'_3=\zeta(\boldsymbol{x}'_\parallel)}L(\boldsymbol{x}'_\parallel|\omega), \tag{2.18}$$

where $\theta(x)$ is the Heaviside step-function and the source function $L(\boldsymbol{x}_\parallel|\omega)$ is defined by:

$$L(\boldsymbol{x}_\parallel|\omega) = [\frac{\partial}{\partial N}\psi(\boldsymbol{x}_\parallel|\omega)]\Big|_{x_3=\zeta(\boldsymbol{x}_\parallel)}. \tag{2.19}$$

The incident part of the wave is assumed to be a plane wave and can be written: $\psi(\boldsymbol{x}|\omega)_{\mathrm{inc}} = \exp(i\boldsymbol{k}_\parallel\cdot\boldsymbol{x}_\parallel - i\alpha_0(k_\parallel)x_3)$. Under the condition $x_3 \gg \zeta(\boldsymbol{x}_\parallel)$, the last term in Eq. (2.18) representing the scattered field, can be written:

$$\psi(\boldsymbol{x}|\omega)_{\mathrm{sc}} = \int \frac{\mathrm{d}^2q_\parallel}{(2\pi)^2}R_D(\boldsymbol{q}_\parallel|\boldsymbol{k}_\parallel)\exp(i\boldsymbol{q}_\parallel\cdot\boldsymbol{x}_\parallel + i\alpha_0(q_\parallel)x_3), \tag{2.20}$$

with scattering amplitude

$$R_D(\boldsymbol{q}_\parallel|\boldsymbol{k}_\parallel) = -\frac{i}{2\alpha_0(q_\parallel)}\int \mathrm{d}^2x_\parallel L(\boldsymbol{x}_\parallel|\omega)\exp(-i\boldsymbol{q}_\parallel\cdot\boldsymbol{x}_\parallel - i\alpha_0(q_\parallel)\zeta(\boldsymbol{x}_\parallel)). \tag{2.21}$$

2.2.1 Kirchhoff approximation

The Kirchhoff approximation constitutes that the scattering takes place as reflections from the tangent-plane at each point of the surface. It is a single-scattering approximation, that is expected to hold for weakly rough surfaces. It's validity in terms of the parameters used in describing Gaussian surfaces, will be adressed in section 2.4.

In general, the source function $L(\boldsymbol{x}_\parallel|\omega)$ satisfies an integral equation that is complicated to solve. Under the Kirchhoff approximation, $L(\boldsymbol{x}_\parallel|\omega)$ simplifies to:

$$\begin{aligned} L(\boldsymbol{x}_\parallel|\omega) =& 2\left(-\frac{\partial\zeta(\boldsymbol{x}_\parallel)}{\partial x_1}\frac{\partial}{\partial x_1} - \frac{\partial\zeta(\boldsymbol{x}_\parallel)}{\partial x_2}\frac{\partial}{\partial x_2} + \frac{\partial}{\partial x_3}\right)\psi(\boldsymbol{x}_\parallel|\omega)_{\text{inc}}\Big|_{x_3=\zeta(\boldsymbol{x}_\parallel)} \\ =& -2i\left(k_1\frac{\partial\zeta(\boldsymbol{x}_\parallel)}{\partial x_1} + k_2\frac{\partial\zeta(\boldsymbol{x}_\parallel)}{\partial x_2} + \alpha_0(k_\parallel)\right)\exp(i\boldsymbol{k}_\parallel\cdot\boldsymbol{x}_\parallel - i\alpha_0(k_\parallel)\zeta(\boldsymbol{x}_\parallel)). \end{aligned} \tag{2.22}$$

Applying the expression to the scattering amplitude R_D and rewriting so that the surface derivatives no longer appears, one gets:

$$\begin{aligned} R_D(\boldsymbol{q}_\parallel|\boldsymbol{k}_\parallel) =& -\frac{(\omega/c)^2 + \alpha_0(q_\parallel)\alpha_0(k_\parallel) - \boldsymbol{q}_\parallel\cdot\boldsymbol{k}_\parallel}{\alpha_0(q_\parallel)[\alpha_0(q_\parallel)+\alpha_0(k_\parallel)]} \\ &\times\int \mathrm{d}^2x_\parallel \exp(-i(\boldsymbol{q}_\parallel-\boldsymbol{k}_\parallel)\cdot\boldsymbol{x}_\parallel)\exp(-i(\alpha_0(q_\parallel)+\alpha_0(k_\parallel))\zeta(\boldsymbol{x}_\parallel)). \end{aligned} \tag{2.23}$$

It is also worth noting at this point that if the Neumann boundary condition was applied instead of the Dirichlet condition, it can be shown that the scattering amplitude under the Kirchhoff approximation would become: $R_N = -R_D$. In the far field and under the Neumann condition, the scattered field can be expressed from Eq. (2.20), with R_N taking the place of of R_D. This means that the field will be the same in the far-zone, except for a phase shift that is irrelevant for the physical quantities that will be discussed.

2.3 Mean differential reflection coefficient(MDRC)

The differential reflection coefficient is defined so that $(\frac{\partial R}{\partial\Omega_s})\mathrm{d}\Omega_s$ is the fraction of total time-averaged incident flux that is scattered into a solid angle element $\mathrm{d}\Omega_s$ around a given scattering direction as $\mathrm{d}\Omega_s$ goes to zero. By calculating the energy flux across the area of the surface in the x_1x_2-plane for the incident and scattered wave, it can be shown that the differential reflection coefficient can be written:

$$\frac{\partial R}{\partial\Omega_S} = \frac{1}{S}\left(\frac{\omega}{2\pi c}\right)^2\frac{\cos^2\theta_\mathrm{s}}{\cos\theta_0}|R(\boldsymbol{q}_\parallel|\boldsymbol{k}_\parallel)|^2. \tag{2.24}$$

Taking the mean of the expression, one ends up with:

$$\left\langle\frac{\partial R}{\partial\Omega_S}\right\rangle = \frac{1}{S}\left(\frac{\omega}{2\pi c}\right)^2\frac{\cos^2\theta_\mathrm{s}}{\cos\theta_0}\langle|R(\boldsymbol{q}_\parallel|\boldsymbol{k}_\parallel)|^2\rangle. \tag{2.25}$$

Plugging in the approximation for $R(\boldsymbol{q}_\parallel|\boldsymbol{k}_\parallel)$ from equation 2.23, the expression for the mean differential reflection coefficient(MDRC) becomes:

$$\begin{aligned}\left\langle \frac{\partial R}{\partial \Omega_s} \right\rangle =& \frac{1}{S}\frac{1}{4\pi^2\cos(\theta_0)}\frac{\left[(\omega/c)^2+\alpha_0(q_\parallel)\alpha_0(k_\parallel)-\boldsymbol{q}_\parallel\cdot\boldsymbol{k}_\parallel\right]^2}{\left[\alpha_0(q_\parallel)+\alpha_0(k_\parallel)\right]^2} \\ &\times\int \mathrm{d}^2x_\parallel \int \mathrm{d}^2x'_\parallel \exp\{-i(\boldsymbol{q}_\parallel-\boldsymbol{k}_\parallel)\cdot(\boldsymbol{x}_\parallel-\boldsymbol{x}'_\parallel)\} \\ &\times\left\langle \exp\{-i(\omega/c)(\alpha_0(q_\parallel)+\alpha_0(k_\parallel))(\zeta(\boldsymbol{x}_\parallel)-\zeta(\boldsymbol{x}'_\parallel))\}\right\rangle .\end{aligned} \tag{2.26}$$

2.4 Gaussian random surfaces

The height $\zeta(\boldsymbol{x}_\parallel)$ is assumed to be a zero-mean Gaussian stationary process defined by:

$$\langle\zeta(\boldsymbol{x}_\parallel)\rangle = 0 \tag{2.27}$$

$$\langle\zeta(\boldsymbol{x}_\parallel)\zeta(\boldsymbol{x}'_\parallel)\rangle = \delta^2 W(\boldsymbol{x}_\parallel-\boldsymbol{x}'_\parallel). \tag{2.28}$$

The parameter δ denotes the root mean square of the surface roughness and $W(\boldsymbol{x}_\parallel-\boldsymbol{x}'_\parallel)$ is the height-height correlation function normalized so that $W(0)=1$.

Gaussian random surfaces have height-distributions given by:

$$p(\zeta) = \frac{1}{\sqrt{2\pi\delta^2}}\exp\left(-\frac{\zeta^2}{2\delta^2}\right). \tag{2.29}$$

Assuming an isotropic height-distribution the two-point height probability function is:[10]

$$p_2(\zeta,\zeta',\boldsymbol{x}'_\parallel-\boldsymbol{x}_\parallel) = \frac{1}{2\pi\delta^2\sqrt{[1-W^2(\boldsymbol{x}'_\parallel-\boldsymbol{x}_\parallel)]}}\exp\left(\frac{\zeta^2+\zeta'^2-2\zeta\zeta' W(\boldsymbol{x}'_\parallel-\boldsymbol{x}_\parallel)}{2\delta^2[1-W^2(\boldsymbol{x}'_\parallel-\boldsymbol{x}_\parallel)]}\right). \tag{2.30}$$

2.5 Validity of the Kirchhoff approximation

Having established the description of Gaussian randomly rough surfaces, the validity of the Kirchhoff approximation can be discussed based on the relevant physical quantities describing the surface. Historically, the most used criterion is $\frac{2\pi}{\lambda}r_c\cos^3\theta_0 \gg 1$, with r_c being the local radius of curvature[15]. It determines the validity of the assumption of the scattering taking place from tangential planes of the surface. This criterion does not, however, consider global effects such as multiple scattering effects and shadowing effects that take place at large angles. The criterion:

$$\frac{\delta^2}{a} \leq 0.2\lambda, \tag{2.31}$$

given $\theta_0 = 0°$ has been suggested as a more practical criterion for Gaussian correlation functions by Shi et al.[11] It is based upon the error in the peak MDRC being less than 1dB at normal incidence. It also was suggested that the scattering angle should also not exceed $\approx 70°$ for this formula to be valid. Increasing the angle of incidence is thought to increase the range of validity, since it reduces the Rayleigh parameter $R = \frac{2\pi}{\lambda}\delta\cos\theta_0$, which effectively reduces the roughness somewhat. This can be understood later by inspecting the equations for the MDRC. This is

however only true as long as the angle of incidence is modest, $\theta_0 \leq 30°$. For large incident and scattering angles, the Kirchhoff approximation becomes invalid due to lacking to take into account multiple scattering. An important part of the lacking multiple scattering effects is shadowing. In our model, the entire surface will be illuminated by the incident beam. In reality, parts of the surface will be shadowed by others for large angles θ_0.[3]

In this thesis however, these criteria will not be followed strictly. Instead, the criterion that the scattered energy equals that of the incident will be used as a guideline.

2.6 Summary

In summary, some remarks on the model:

- The wave is scalar.
- The incident beam is a plane wave.
- The scattering surface is mathematically a hard wall(No transmission), and has infinite area.
- The scattering surface has a Gaussian height-distribution.
- The Kirchhoff approximation has been made, neglecting multiple scattering and putting constraints on what parameters δ/λ and a/λ can be used.
- The Neumann and Dirichlet boundary conditions gives the same physical results.
- Three input parameters for isotropic correlation functions: θ_0, a/λ, δ/λ (ϕ_0 is redundant in this case). Five for anisotropic: θ_0, a_1/λ, a_2/λ,δ/λ, ϕ_0.

The fact that the model can be expressed in terms of a/λ and δ/λ is perhaps not immediately apparent when looking at the equations as they stand in this section. It can be shown for instance by changing integration variables in Eq. (4.3) to $y_1 = \frac{u_{\parallel 1}}{a_1}$ and $y_2 = \frac{u_{\parallel 2}}{a_2}$. Then one can see that every factor δ, a_1, a_2 (or simply a) can be moved next to a factor $\alpha_0(...)$, $q_\parallel$, $k_\parallel$ or (ω/c) who carry a $1/\lambda$ dependence.

Chapter 3

Definition of haze

Haze and gloss are terms that are often used in the optical industry to quantify the visual appearance of materials. Gloss is a measure of the fraction of reflected light intensity that is directed around the specular direction. Haze is a complimentary quantity that is a measure of the fraction of the reflected light intensity that is directed into other directions than those around the specular. Having defined the MDRC, a definition of these quantities for scattering from two-dimensionally surfaces can now be made.

There is no standard definition for haze and gloss in the industry. Nor is there a standard for how far away from the specular direction the reflected light can go and still be *around* it. In this thesis, these directions are defined as the directions where the angle between the scattered momentum vector and a vector pointing in the specular direction is less than some limit angle Θ_{lim}. The definition builds on the definition that has often has been used previously in the theoretical study of gloss from 1D-surfaces[13]. One can also talk of gloss and haze in transmission, but that will not be discussed in this thesis, since the model used here only allows for reflection. Yet, the following definitions are valid for haze/gloss in reflection for all surface models

The total time-averaged flux of reflected light is defined as the surface integral of the MDRC over all scattering directions:

$$\mathcal{U} = \int_{\theta_s<\pi/2} \left\langle \frac{\partial R}{\partial \Omega_s} \right\rangle \mathrm{d}\Omega_s = \int_{|\boldsymbol{q}_\parallel|<(\omega/c)} \frac{1}{(\omega/c)\alpha_0(q_\parallel)} \left\langle \frac{\partial R}{\partial \Omega_s} \right\rangle \mathrm{d}^2 q_\parallel. \tag{3.1}$$

Haze, being defined as the fraction of this flux going into directions not around the specular, can be defined as:

$$\mathcal{H}(\Theta_{\text{lim}}) = \frac{1}{\mathcal{U}} \int_{\Delta\Omega_{\mathcal{H}}} \left\langle \frac{\partial R}{\partial \Omega_s} \right\rangle \mathrm{d}\Omega_s = \frac{1}{\mathcal{U}} \int_{A_{\mathcal{H}}} \frac{1}{(\omega/c)\alpha_0(q_\parallel)} \left\langle \frac{\partial R}{\partial \Omega_s} \right\rangle \mathrm{d}^2 q_\parallel. \tag{3.2}$$

The area $A_{\mathcal{H}}$ has the outer bound $|\boldsymbol{q}_\parallel| = (\omega/c)$ and inner bound defined by the curve where the the angle between the scattered momentum vector and a vector pointing in the specular direction is Θ_{lim}: $\boldsymbol{q}(\boldsymbol{q}_\parallel) \cdot \boldsymbol{q}(\boldsymbol{k}_\parallel) = (\omega/c)^2 \cos(\Theta_{\text{lim}})$.

Gloss can be defined as:

$$\mathcal{G}(\Theta_{\text{lim}}) = \frac{1}{\mathcal{U}} \int_{\Delta\Omega_{\mathcal{G}}} \left\langle \frac{\partial R}{\partial \Omega_s} \right\rangle \mathrm{d}\Omega_s = \frac{1}{\mathcal{U}} \int_{A_{\mathcal{G}}} \frac{1}{(\omega/c)\alpha_0(q_\parallel)} \left\langle \frac{\partial R}{\partial \Omega_s} \right\rangle \mathrm{d}^2 q_\parallel. \tag{3.3}$$

The area $A_{\mathcal{G}}$ is the area enclosed by $\boldsymbol{q}(\boldsymbol{q}_\parallel)\cdot\boldsymbol{q}(\boldsymbol{k}_\parallel) = (\omega/c)^2 \cos(\Theta_{\text{lim}})$. This is the same curve as the inner boundary for the area $A_{\mathcal{H}}$. Using that fact, the expression for haze can be rewritten:

$$\mathcal{H}(\Theta_{\text{lim}}) = \frac{1}{\mathcal{U}}\left(\mathcal{U} - \int_{A_\mathcal{G}} \frac{1}{(\omega/c)\alpha_0(q_\parallel)} \left\langle \frac{\partial R}{\partial \Omega_s} \right\rangle \mathrm{d}^2 q_\parallel \right) = 1 - \mathcal{G}(\Theta_{\text{lim}}). \tag{3.4}$$

By changing to a coordinate system rotated ϕ_0 about the x_3-axis, so that $k_\parallel$ lies along the x_1'-axis, it can be shown that the curve enclosing $A_\mathcal{G}$ is an ellipse.

$$\begin{bmatrix} x_1' \\ x_2' \\ x_3' \end{bmatrix} = \begin{bmatrix} \cos\phi_0 & \sin\phi_0 & 0 \\ -\sin\phi_0 & \cos\phi_0 & 0 \\ 0 & 0 & 1 \end{bmatrix} \begin{bmatrix} x_1 \\ x_2 \\ x_3 \end{bmatrix}. \tag{3.5}$$

The edge of $A_\mathcal{G}$ satisfies the equation:

$$\boldsymbol{q}(\boldsymbol{q}_\parallel) \cdot \boldsymbol{q}(\boldsymbol{k}_\parallel) = (\omega/c)^2 \cos(\Theta_{\text{lim}}), \tag{3.6}$$

which in the new rotated coordinate system can be written:

$$\begin{gathered} q_1' k_\parallel + \alpha_0(q_\parallel)\alpha_0(k_\parallel) = (\omega/c)^2 \cos(\Theta_{\text{lim}}) \\ \Downarrow \\ (q_1' k_\parallel - (\omega/c)^2 \cos(\Theta_{\text{lim}}))^2 = \alpha_0^2(k_\parallel)((\omega/c)^2 - q_1'^2 - q_2'^2). \end{gathered}$$

This can be rewritten to the form:

$$\frac{(q_1' - k_\parallel \cos(\Theta_{\text{lim}}))^2}{(\alpha_0(k_\parallel)\sin(\Theta_{\text{lim}}))^2} + \frac{q_2'^2}{((\omega/c)\sin(\Theta_{\text{lim}}))^2} = 1, \tag{3.7}$$

which is recognized as the expression for an ellipse.

From Eq. (3.7) it can be seen that $A_\mathcal{G}$ is the area of an ellipse with origin at $(q_1', q_2') = (k_\parallel \cos(\Theta_{\text{lim}}), 0)$ or $(q_1, q_2) = k_\parallel \cos(\Theta_{\text{lim}})(\cos\phi_0, \sin\phi_0)$. The minor axis lies along the x_1'-axis(Or similarly the line $x_2 = \frac{k_2}{k_1} x_1$) and has length $L_{\text{min}} = 2\alpha_0(k_\parallel)\sin(\Theta_{\text{lim}})$. The major axis has length $L_{\text{maj}} = 2(\omega/c)\sin(\Theta_{\text{lim}})$.

Figure 3.1 shows the integration area $A_\mathcal{G}$ when $\theta_0 = 70°$ and $\Theta_{lim} = 15°$.For such large values of θ_0 and Θ_{lim} it becomes apparent that $A_\mathcal{G}$ is an ellipse and that its origin is not at the point $(q_1', q_2') = (k_\parallel, 0)$, but rather $(q_1', q_2') = (k_\parallel \cos(\Theta_{\text{lim}}), 0)$. This is helpful to bear in mind, since we will do the approximation of the shape of $A_\mathcal{G}$ being circular when deriving approximate expressions for haze.

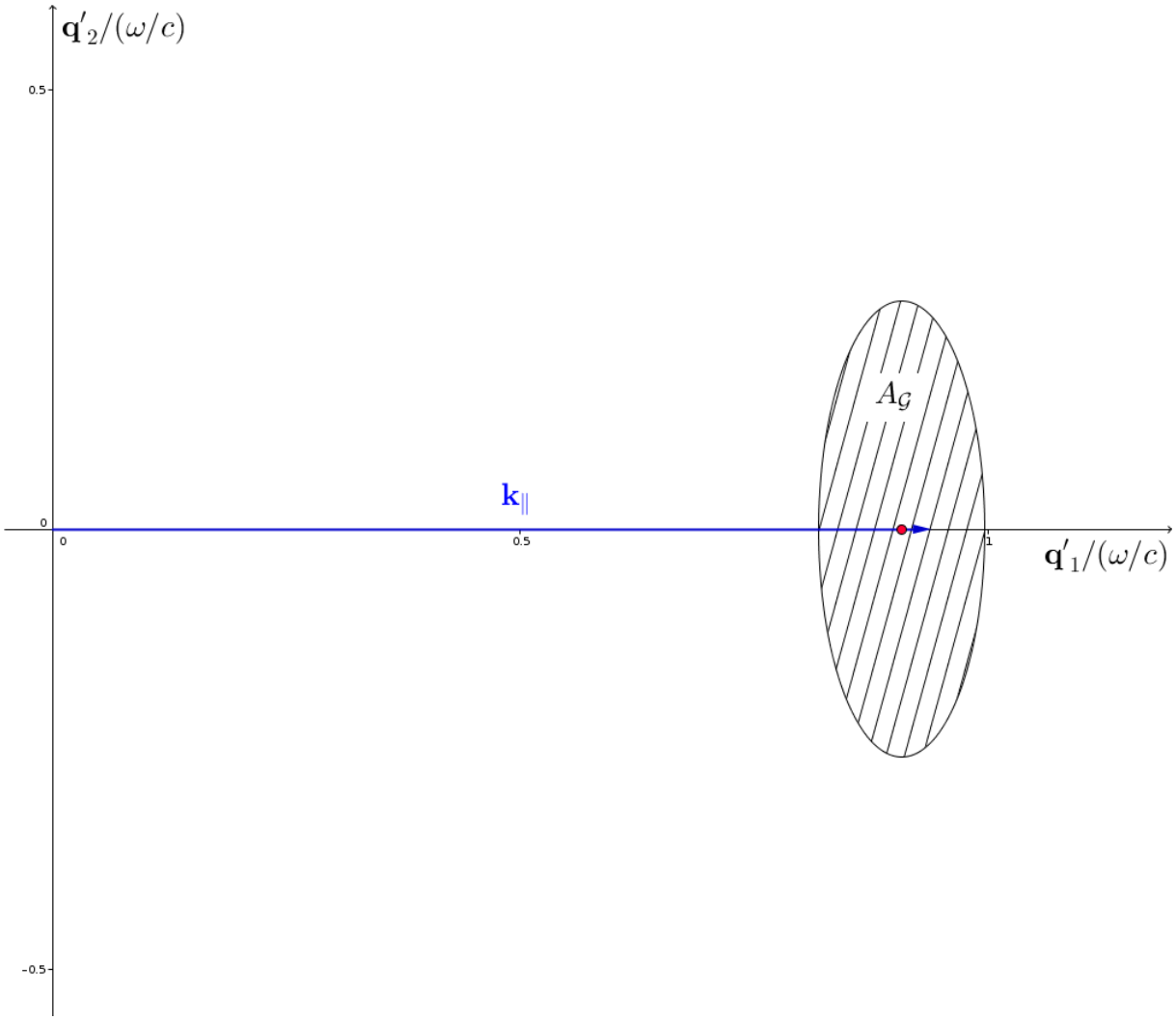

Figure 3.1: $A_{\mathcal{G}}$ when $\Theta_{\text{lim}} = 15°$ and $\theta_0 = 70°$ in the rotated coordinate system $x'_1x'_2$. The red dot marks the origin of the ellipse.

Chapter 4

Expressions for MDRC

Under the assumption that $\zeta(\boldsymbol{x}_\parallel)$ is a Gaussian, isotropic and stationary process, the factor $\langle \exp[-i(\omega/c)(\alpha_0(q_\parallel)+\alpha_0(k_\parallel))(\zeta(\boldsymbol{x}_\parallel)-\zeta(\boldsymbol{x}'_\parallel))]\rangle$ from the expression for the MDRC as given by Eq. 2.26 can be calculated analytically by using the two-point height probability function given in Eq. (2.30) to obtain:

$$\begin{aligned}
&\langle \exp[-i(\omega/c)(\alpha_0(q_\parallel)+\alpha_0(k_\parallel))(\zeta(\boldsymbol{x}_\parallel)-\zeta(\boldsymbol{x}'_\parallel))]\rangle \\
&\qquad = \int_{-\infty}^{\infty}\int_{-\infty}^{\infty} \exp[-i(\omega/c)(\alpha_0(q_\parallel)+\alpha_0(k_\parallel))(\zeta-\zeta')]p_2(\zeta,\zeta',{\boldsymbol{x}_\parallel}'-\boldsymbol{x}_\parallel)d\zeta d\zeta' \\
&\qquad = \exp[-\delta^2(\alpha_0(q_\parallel)+\alpha_0(k_\parallel))^2(1-W({\boldsymbol{x}_\parallel}'-\boldsymbol{x}_\parallel))].
\end{aligned} \tag{4.1}$$

Plugging this expression into the formula for the MDRC as given by Eq. (2.26) and dubbing $\boldsymbol{u}_\parallel = {\boldsymbol{x}_\parallel}'-\boldsymbol{x}_\parallel$, one obtains an expression for the MDRC for a surface with a Gaussian, stationary and isotropic height distribution:

$$\begin{aligned}
\left\langle \frac{\partial R}{\partial \Omega_s} \right\rangle = &\frac{1}{S}\frac{\exp[-(\alpha_0(q_\parallel)+\alpha_0(k_\parallel))^2\delta^2]}{4\pi^2\cos(\theta_0)}\frac{\left[(\omega/c)^2+\alpha_0(q_\parallel)\alpha_0(k_\parallel)-\boldsymbol{q}_\parallel\cdot\boldsymbol{k}_\parallel\right]^2}{\left[\alpha_0(q_\parallel)+\alpha_0(k_\parallel)\right]^2} \\
&\times\int \mathrm{d}^2x_\parallel \int \mathrm{d}^2x'_\parallel \exp[-i(\boldsymbol{q}_\parallel-\boldsymbol{k}_\parallel)\cdot\boldsymbol{u}_\parallel]\exp[(\alpha_0(q_\parallel)+\alpha_0(k_\parallel))^2\delta^2 W(\boldsymbol{u}_\parallel)].
\end{aligned} \tag{4.2}$$

Changing the coordinate of the inner integration to $\boldsymbol{u}_\parallel$, the outer integral simply amounts to a factor S and the equation becomes:

$$\begin{aligned}
\left\langle \frac{\partial R}{\partial \Omega_s} \right\rangle = &\frac{\exp[-(\alpha_0(q_\parallel)+\alpha_0(k_\parallel))^2\delta^2]}{4\pi^2\cos(\theta_0)}\frac{\left[(\omega/c)^2+\alpha_0(q_\parallel)\alpha_0(k_\parallel)-\boldsymbol{q}_\parallel\cdot\boldsymbol{k}_\parallel\right]^2}{\left[\alpha_0(q_\parallel)+\alpha_0(k_\parallel)\right]^2} \\
&\times\int \mathrm{d}^2u_\parallel \exp[-i(\boldsymbol{q}_\parallel-\boldsymbol{k}_\parallel)\cdot\boldsymbol{u}_\parallel]\exp[(\alpha_0(q_\parallel)+\alpha_0(k_\parallel))^2\delta^2 W(\boldsymbol{u}_\parallel)].
\end{aligned} \tag{4.3}$$

4.1 Gaussian and exponential correlation functions

Writing out the last exponential function of Eq. (4.3) as its series representation, the equation becomes:

$$\begin{aligned}\left\langle \frac{\partial R}{\partial \Omega_s} \right\rangle =& \frac{\exp[-(\alpha_0(q_\parallel)+\alpha_0(k_\parallel))^2\delta^2)}{4\pi^2\cos(\theta_0)} \frac{\left[(\omega/c)^2+\alpha_0(q_\parallel]\alpha_0(k_\parallel)-\boldsymbol{q}_\parallel\cdot\boldsymbol{k}_\parallel\right]^2}{\left[\alpha_0(q_\parallel)+\alpha_0(k_\parallel)\right]^2} \\ & \sum_{n=0}^{\infty}\frac{[(\alpha_0(q_\parallel)+\alpha_0(k_\parallel))\delta]^{2n}}{n!}\mathcal{F}[W^n(\boldsymbol{u}_\parallel)](\boldsymbol{q}_\parallel-\boldsymbol{k}_\parallel).\end{aligned} \tag{4.4}$$

Here we have introduced $\mathcal{F}[W^n(\boldsymbol{u}_\parallel)](\boldsymbol{q}_\parallel-\boldsymbol{k}_\parallel)$ as the two dimensional fourier transform of the n'th power of the correlation function:

$$\mathcal{F}[W^n(\boldsymbol{u}_\parallel)](\boldsymbol{q}_\parallel-\boldsymbol{k}_\parallel)=\int \mathrm{d}^2u_\parallel W^n(\boldsymbol{u}_\parallel)\exp[-i(\boldsymbol{q}_\parallel-\boldsymbol{k}_\parallel)\cdot\boldsymbol{u}_\parallel]. \tag{4.5}$$

For Gaussian isotropic-, Gaussian anisotropic-, exponential- and other correlation functions where an analyitcal expression for this Fourier transform can be found, the series form of the MDRC as given in Eq. (4.4) is convenient.

The zero'th component of the series representation of the MDRC corresponds to the coherent component of the scattered wave. Independent of correlation function it is:

$$\boxed{\begin{aligned}\left\langle \frac{\partial R}{\partial \Omega_s} \right\rangle_{\text{coh}} =& \frac{\exp[-(\alpha_0(q_\parallel)+\alpha_0(k_\parallel))^2\delta^2]}{4\pi^2\cos(\theta_0)} \frac{\left[(\omega/c)^2+\alpha_0(q_\parallel)\alpha_0(k_\parallel)-\boldsymbol{q}_\parallel\cdot\boldsymbol{k}_\parallel\right]^2}{\left[\alpha_0(q_\parallel)+\alpha_0(k_\parallel)\right]^2} \\ & \times(2\pi)^2\delta(\boldsymbol{q}_\parallel-\boldsymbol{k}_\parallel).\end{aligned}} \tag{4.6}$$

The incoherent part of the MDRC is:

$$\boxed{\begin{aligned}\left\langle \frac{\partial R}{\partial \Omega_s} \right\rangle_{\text{incoh}} =& \frac{\exp[-(\alpha_0(q_\parallel)+\alpha_0(k_\parallel))^2\delta^2]}{4\pi^2\cos(\theta_0)} \frac{\left[(\omega/c)^2+\alpha_0(q_\parallel)\alpha_0(k_\parallel)-\boldsymbol{q}_\parallel\cdot\boldsymbol{k}_\parallel\right]^2}{\left[\alpha_0(q_\parallel)+\alpha_0(k_\parallel)\right]^2} \\ & \times\sum_{n=1}^{\infty}\frac{[(\alpha_0(q_\parallel)+\alpha_0(k_\parallel))\delta]^{2n}}{n!}\mathcal{F}[W^n(\boldsymbol{u}_\parallel)](\boldsymbol{q}_\parallel-\boldsymbol{k}_\parallel).\end{aligned}} \tag{4.7}$$

Due to the factor $1/n!$, the sum in Eq. (4.7) is expected to converge rapidly, especially when δ/λ is small.For the correlation functions that will be studied in this thesis, the Fourier transforms, $\mathcal{F}[W^n(\boldsymbol{u}_\parallel)](\boldsymbol{q}_\parallel-\boldsymbol{k}_\parallel)$, are given in Table 4.1.

4.2 Isotropic correlation function

Although only the previously mentioned correlation functions will be discussed in this thesis, the MDRC for a general isotropic correlation function will be given for completeness. For such correlation functions, where no analytic expression for fourier transform of $W^n(\boldsymbol{u}_\parallel)$ can be found, some progress can still be made in the sense that the complex 2d-integral in Eq. (4.3) can be

Table 4.1: Fourier transforms of different correlation functions to the n'th power.

	$W(\boldsymbol{u}_\parallel)$	$\mathcal{F}[W^n(\boldsymbol{u}_\parallel)](\boldsymbol{Q}_\parallel)$
Gaussian	$\exp\left(-\frac{u_\parallel^2}{a^2}\right)$	$\frac{\pi a^2}{n}\exp\left(-\frac{Q_\parallel^2 a^2}{4n}\right)$
Gaussian anisotropic	$\exp\left(-\left(\frac{u_1^2}{a_1^2}+\frac{u_2^2}{a_2^2}\right)\right)$	$\frac{\pi a_1 a_2}{n}\exp\left(-\left(\frac{Q_1^2 a_1^2}{4n}+\frac{Q_2^2 a_2^2}{4n}\right)\right)$
Exponential	$\exp\left(-\frac{u_\parallel}{a}\right)$	$2\pi a^2 n(n^2+Q_\parallel^2 a^2)^{-3/2}$

reduced to a real 1d-integral. The incoherent part of the MDRC given as given by Eq. (4.3) is:

$$\left\langle \frac{\partial R}{\partial \Omega_s} \right\rangle_{\text{incoh}} = \frac{\exp[-(\alpha_0(q_\parallel)+\alpha_0(k_\parallel))^2\delta^2]}{4\pi^2\cos(\theta_0)} \frac{\left[(\omega/c)^2+\alpha_0(q_\parallel)\alpha_0(k_\parallel)-\boldsymbol{q}_\parallel\cdot\boldsymbol{k}_\parallel\right]^2}{\left[\alpha_0(q_\parallel)+\alpha_0(k_\parallel)\right]^2} \times \int \mathrm{d}^2u_\parallel \exp[-i(\boldsymbol{q}_\parallel-\boldsymbol{k}_\parallel)\cdot\boldsymbol{u}_\parallel]\left[\exp[(\alpha_0(q_\parallel)+\alpha_0(k_\parallel))^2\delta^2 W(u_\parallel)]-1\right]. \tag{4.8}$$

The coherent part is still given by Eq. (4.6). Dubbing $f(u_\parallel) = \left(\exp((\alpha_0(q_\parallel)+\alpha_0(k_\parallel))^2\delta^2 W(u_\parallel))-1\right)$ for readability, the integral in Eq. (4.8), can be rewritten:

$$\begin{aligned} I(|\boldsymbol{q}_\parallel-\boldsymbol{k}_\parallel|) &= \int \mathrm{d}^2u_\parallel \exp[-i(\boldsymbol{q}_\parallel-\boldsymbol{k}_\parallel)\cdot\boldsymbol{u}_\parallel]f(u_\parallel) \\ &= \int_0^\infty \mathrm{d}u_\parallel u_\parallel f(u_\parallel)\int_0^{2\pi}\mathrm{d}\Theta_\mathrm{u}\exp[-i|\boldsymbol{q}_\parallel-\boldsymbol{k}_\parallel|u_\parallel\cos\Theta_\mathrm{u}] \\ &= 2\pi\int_0^\infty \mathrm{d}u_\parallel u_\parallel f(u_\parallel)J_0(|\boldsymbol{q}_\parallel-\boldsymbol{k}_\parallel|u_\parallel). \end{aligned} \tag{4.9}$$

Here J_0 denotes the zero'th order Bessel function of the first kind. The integral $I(|\boldsymbol{q}_\parallel-\boldsymbol{k}_\parallel|)/(2\pi)$ is also referred to as the Hankel transform of $f(u_\parallel)$. This is an oscillating integral that can be computed numerically. Moreover, there exists numerical methods for computing a discrete Hankel transform which could also be used.

For a general isotropic correlation function:

$$\boxed{\left\langle \frac{\partial R}{\partial \Omega_s} \right\rangle_{\text{incoh}} = \frac{\exp[-(\alpha_0(q_\parallel)+\alpha_0(k_\parallel))^2\delta^2]}{4\pi^2\cos(\theta_0)} \frac{\left[(\omega/c)^2+\alpha_0(q_\parallel)\alpha_0(k_\parallel)-\boldsymbol{q}_\parallel\cdot\boldsymbol{k}_\parallel\right]^2}{\left[\alpha_0(q_\parallel)+\alpha_0(k_\parallel)\right]^2} \times 2\pi\int_0^\infty \mathrm{d}u_\parallel u_\parallel\left[\exp[(\alpha_0(q_\parallel)+\alpha_0(k_\parallel))^2\delta^2 W(u_\parallel)]-1\right]J_0(|\boldsymbol{q}_\parallel-\boldsymbol{k}_\parallel|u_\parallel).} \tag{4.10}$$

Chapter 5

Approximate expressions for haze

In deriving the following expression for haze, three additional approximations has been made:

1. $\mathcal{U} = 1$. The total scattered energy is assumed to be equal to the incident energy.

2. $A_{\mathcal{G}}$ is circular. For all the approximate expressions this assumption is made, except for the one for a general anisotropic correlation function, where it can be evaded. The length of the minor axis of $A_{\mathcal{G}}$ goes like $\propto (1 - \cos\theta_0)$, and should thus the contraction not be too prominent for modest angles of incidence.

3. Except for the factors $\mathcal{F}[W^n(\boldsymbol{u}_\parallel)](\boldsymbol{Q}_\parallel)$, the MDRC is approximated by taking $\boldsymbol{q}_\parallel = \boldsymbol{k}_\parallel$. Since the haze is calculated by integrating over a relatively small area around $\boldsymbol{k}_\parallel$ and that $\mathcal{F}[W^n(\boldsymbol{u}_\parallel)](\boldsymbol{Q}_\parallel)$ typically is more rapidly changing than the other parts of the MDRC, this is expected to give decent results. In the more general approximate expressions that will be given, this corresponds to putting $\boldsymbol{q}_\parallel = \boldsymbol{k}_\parallel$ everywhere except for the oscillating exponential function in Eq. (4.3)

Before getting into deriving approximate expressions for haze, it can often be helpful to notice the contribution to the haze from the coherent part of the scattered wave. This result is independent of the approximations made above except for $\mathcal{U} = 1$ and independent of what correlation function is assumed. The coherent contribution reduces the value of the haze and and gives an upper bound on what the final value can be. When δ/λ is low, this reduction becomes significant.

$$\mathcal{H} < 1 - \exp(-4\alpha_0^2(k_\parallel)\delta^2). \tag{5.1}$$

When δ/λ is very small, the haze can be approximated by the coherent contribution only.

Also, some points should be made on the radius of $A_{\mathcal{G}}$. When $\theta_0 = 0°$, the radius is $\Delta Q = (\omega/c)\sin(\Theta_{\text{lim}})$. As stated earlier, the integration should not be carried out over an circular area in the q_1q_2-plane when the angle of incidence is non-zero. Rather it should be carried out over an ellipse with area $A = \pi(L_{\text{min}}/2)(L_{\text{maj}}/2) = \pi(\omega/c)^2\sin^2(\Theta_{\text{lim}})\cos\theta_0$. Choosing:

$$\Delta Q = (\omega/c)\sin(\Theta_{\text{lim}})\sqrt{\cos\theta_0}, \tag{5.2}$$

will give an integration area of correct magnitude, though the shape is still not correct. There is however no correct choice for this radius and other smarter choices could be made, giving a better behaviour for large θ_0.

5.1 Gaussian and exponential correlation functions

The haze as given by the expression $\mathcal{H} = 1 - \mathcal{G}$ can be rewritten on the following form, when the incoherent part of the MDRC is on the series form given in Eq. (4.4) and the three approximations mentioned before are made:

$$\boxed{\mathcal{H} \approx 1 - \exp(-4\alpha_0^2(k_\parallel)\delta^2)\left[1 + \sum_{n=1}^{\infty} \frac{(2\alpha_0(k_\parallel)\delta)^{2n}}{n!} \int_{A_\mathcal{G}} \mathcal{F}[W^n(\boldsymbol{u}_\parallel)](\boldsymbol{Q}_\parallel)\frac{\mathrm{d}^2 Q_\parallel}{(2\pi)^2}\right].} \tag{5.3}$$

When the approximation of a circular $A_\mathcal{G}$ is made, convenient, analytical expressions are found for the integrals for the Gaussian and exponential correlation functions. For the Gaussian anisotropic correlation function, the integrals over $A_\mathcal{G}$ is reduced to 1d-integrals. The results are found in Table 5.1

Table 5.1: Terms used in the approximate analytical expression for haze.

$W(\boldsymbol{u}_\parallel)$	$\int_{A_\mathcal{G}} \mathcal{F}[W^n(\boldsymbol{u}_\parallel)](\boldsymbol{Q}_\parallel)\frac{\mathrm{d}^2 Q_\parallel}{(2\pi)^2}$
$\exp(-\frac{u_\parallel^2}{a^2})$	$1 - \exp(-\frac{a^2\Delta Q_\parallel^2}{4n})$
$\exp(-(\frac{u_1^2}{a_1^2} + \frac{u_2^2}{a_2^2}))$	$a_1 a_2 \int_0^{\Delta Q_\parallel^2/(4n)} \exp(-\frac{a_1^2+a_2^2}{2}u) I_0(\frac{a_1^2-a_2^2}{2}u)\mathrm{d}u$
$\exp(-\frac{u_\parallel}{a})$	$1 - (1 + \frac{a^2\Delta Q^2}{n^2})^{-1/2}$

5.2 General correlation function

The MDRC for a general correlation function is given in Eq. 4.3. Finding a simple approximate analytical expression for haze in this case seems to be out of the question for now. The approximations can, however, be applied anyway to get rid of a couple of integrations. Also, since we have to perform a numerical integration anyways, the requirement of $A_\mathcal{G}$ being circular can be dropped. Assuming $\mathcal{U} = 1$, the haze can be written:

$$\boxed{\mathcal{H} \approx 1 - \exp(-4\alpha_0^2(k_\parallel)\delta^2) - I,} \tag{5.4}$$

where I is the integral of the incoherent part of the MDRC around the specular direction, which we will try to find. Putting $\boldsymbol{q}_\parallel = \boldsymbol{k}_\parallel$ everywhere in the incoherent part of the MDRC given by Eq. (4.3) except for the oscillating exponential function, and integrating, one obtains:

$$I = \frac{\exp(-4\alpha_0^2(k_\parallel)\delta^2)\alpha_0(k_\parallel)}{4\pi^2(\omega/c)} \int \mathrm{d}^2 u_\parallel (\exp(4\alpha_0(k_\parallel)\delta^2 W(\boldsymbol{u}_\parallel)) - 1) \int \mathrm{d}^2 p_\parallel \exp(-i(\boldsymbol{q}_\parallel - \boldsymbol{k}_\parallel)^T \boldsymbol{u}_\parallel). \tag{5.5}$$

The integral is carried out over $x_1' x_2'$, a plane having $\hat{\boldsymbol{x}}_3' \propto \boldsymbol{q}(\boldsymbol{k}_\parallel)$ as its normal vector. In Eq. (5.5), p_i are the components of the scattering vector $\boldsymbol{q}$ in this coordinate system and $\boldsymbol{p}_\parallel$ is $\boldsymbol{q}$ when

the p_3 is zero. The p_3 component is calculated through $p_3 = \alpha_0(p_\parallel)$. In this coordinate system the integration over $A_\mathcal{G}$ can be done over a circular area without making an approximation in calculating haze. Choosing: $\boldsymbol{q}_\parallel = R(A\boldsymbol{p}_\parallel + \boldsymbol{b})$, where:

$$R = \begin{bmatrix} \cos\phi_0 & -\sin\phi_0 \\ \sin\phi_0 & \cos\phi_0 \end{bmatrix}, \tag{5.6}$$

$$A = A^T = \begin{bmatrix} \cos\theta_0 & 0 \\ 0 & 1 \end{bmatrix}, \tag{5.7}$$

$$\boldsymbol{b} = \begin{bmatrix} \alpha_0(p_\parallel)\sin\theta_0 \\ 0 \end{bmatrix} \approx \begin{bmatrix} (\omega/c)\sin\theta_0 \\ 0 \end{bmatrix}. \tag{5.8}$$

The approximation in b comes from that $\boldsymbol{q}_\parallel = \boldsymbol{k}_\parallel$ corresponds to putting $|\boldsymbol{p}_\parallel| = p_\parallel = 0$. The inner integrand in Eq. (5.5) now can be written:

$$\begin{aligned} \exp(-i(\boldsymbol{q}_\parallel - \boldsymbol{k}_\parallel)^T\boldsymbol{u}_\parallel) &= \exp(i((\boldsymbol{k}_\parallel^T R - \boldsymbol{b}^T) - \boldsymbol{p}_\parallel^T A^T)(R^T\boldsymbol{u}_\parallel)) \\ &= \exp(-i\boldsymbol{p}_\parallel^T AR^T\boldsymbol{u}_\parallel) = \exp(-i\boldsymbol{p}_\parallel \cdot (AR^T\boldsymbol{u}_\parallel)). \end{aligned} \tag{5.9}$$

The inner integral over p_1p_2 in Eq. (5.5) can now be evaluated:

$$\begin{aligned} \int \mathrm{d}^2p_\parallel \exp(-i\boldsymbol{p}_\parallel \cdot (AR^T\boldsymbol{u}_\parallel)) &= \int_0^{\Delta p_\parallel} \mathrm{d}p_\parallel p_\parallel \int_0^{2\pi} \mathrm{d}\Theta_p \exp(-ip_\parallel |AR^T\boldsymbol{u}_\parallel| \cos\Theta_p) \\ &= 2\pi \int_0^{\Delta p_\parallel} \mathrm{d}p_\parallel p_\parallel J_0(|AR^T\boldsymbol{u}_\parallel| p_\parallel) \\ &= \frac{2\pi\Delta p_\parallel}{|AR^T\boldsymbol{u}_\parallel|} J_1(|AR^T\boldsymbol{u}_\parallel|\Delta p_\parallel), \end{aligned} \tag{5.10}$$

where $\Delta p_\parallel$ simply is $(\omega/c)\sin(\Theta_{\lim})$. Plugging the expression into Eq. (5.5), and changing to integration variable to $\boldsymbol{v}_\parallel = \Delta p_\parallel AR^T\boldsymbol{u}_\parallel$ we get the following expression for I for a general correlation function:

$$\boxed{I = \frac{\exp(-4\alpha_0^2(k_\parallel)\delta^2)}{2\pi} \int \mathrm{d}^2v_\parallel (\exp(4\alpha_0(k_\parallel)\delta^2 W(M\boldsymbol{v}_\parallel)) - 1)\frac{J_1(v_\parallel)}{v_\parallel},} \tag{5.11}$$

where the matrix M is:

$$M = \frac{1}{\Delta p_\parallel} RA^{-1} = \frac{1}{(\omega/c)\sin(\Theta_{\lim})} \begin{bmatrix} \cos\phi_0/\cos\theta_0 & -\sin\phi_0 \\ \sin\phi_0/\cos\theta_0 & \cos\phi_0 \end{bmatrix}. \tag{5.12}$$

5.3 Isotropic correlation function

If the correlation function is isotropic, i.e. $W(\boldsymbol{u}_\parallel) = W(u_\parallel)$ we might hope to get rid of another integration. This can however, to the authors knowledge, not be done without going back to the assumption that $A_\mathcal{G}$ is circular. In terms of Eq. (5.11), this basicly means that we let:

$$|M\boldsymbol{v}| = \frac{1}{(\omega/c)\sin(\Theta_{\lim})} \sqrt{(\frac{v_1}{\cos\theta_0})^2 + v_2^2} \approx \frac{1}{(\omega/c)\sin(\Theta_{\lim})\sqrt{\cos\theta_0}} |\boldsymbol{v}_\parallel|. \tag{5.13}$$

Going back to doing this approximation and writing:

$$\int \mathrm{d}^2v_\parallel = \int_0^\infty \mathrm{d}v_\parallel v_\parallel \int_0^{2\pi} \mathrm{d}\Theta_v, \tag{5.14}$$

the integration over Θ_v becomes trivial, and we end up with for the following expression for I for an isotropic correlation function:

$$\boxed{I = \exp(-4\alpha_0^2(k_\parallel)\delta^2) \int_0^\infty \mathrm{d}v_\parallel (\exp(4\alpha_0^2(k_\parallel)\delta^2 W(\beta v_\parallel)) - 1) J_1(v_\parallel),} \tag{5.15}$$

where $1/\beta = (\omega/c) \sin\Theta_{\lim} \sqrt{\cos\theta_0}$.

Chapter 6

Methods

6.1 MDRC

Functions calculating the incoherent part of the MDRC for the different correlation functions, as given by Eq. (4.7) and Table 4.1, was implemented in C. These functions are used in code for various purposes such as plotting the MDRC or integrating it numerically over different domains.

6.2 Energy conservation

The coherent part of the MDRC as given by Eq. (4.6) was integrated analytically. Independent of what correlation function is used, its contribution to $\mathcal{U}$ is:

$$\mathcal{U}_{\text{coh}} = \exp(-4\alpha_0^2(k_\parallel)\delta^2) = \exp(-(2R)^2), \tag{6.1}$$

where R is the Rayleigh parameter defined by:

$$R = |\boldsymbol{k}|\delta\cos\theta_0 = \alpha_0(k_\parallel)\delta = 2\pi\frac{\delta}{\lambda}\cos\theta_0. \tag{6.2}$$

The incoherent part of the MDRC was integrated numerically over $|\boldsymbol{q}_\parallel| < (\omega/c)$ using the library *adaptint*[8], an adaptive multi-dimensional integration(cubature) routine, which is an extention to the GSL library. The error tolerance was set to $\epsilon_{\text{rel}} = 10^{-6}$.

6.3 Haze

In determining $\mathcal{H}$, the MDRC needs to be integrated twice. Once over the area in which $q_\parallel < (\omega/c)$ to find $\mathcal{U}$, covered above, and once over the small area around $\boldsymbol{k}_\parallel$, $A_\mathcal{G}$.

In integrating the MDRC over $A_\mathcal{G}$, the integration was carried out by first changing coordinate system to the plane which has a vector pointing in the specular direction(For instance $\boldsymbol{q}(\boldsymbol{k}_\parallel)$) as its normal-vector. This way, the integration area is circular. I.e the integration limits are not

dependent on the integration variables.

$$\begin{aligned} I_{A_\mathcal{G}} &= \int\int \frac{1}{(\omega/c)\alpha_0(\sqrt{p_1^2+p_2^2})} \left\langle \frac{\partial R}{\partial \Omega_S} \right\rangle \mathrm{d}^2 p_\parallel \\ &= \int_0^{2\pi} \int_0^{(\omega/c)\sin(\Theta_{\lim})} \frac{1}{(\omega/c)\alpha_0(p)} \left\langle \frac{\partial R}{\partial \Omega_S} \right\rangle p_\parallel \mathrm{d}p_\parallel \mathrm{d}\Theta. \end{aligned} \tag{6.3}$$

The MDRC can be evaluated by mapping values from p_1p_2-plane to the q_1q_2-plane and inserting them to the MDRC.

$$\begin{bmatrix} q_1 \\ q_2 \end{bmatrix} = \begin{bmatrix} \cos\phi_0 & -\sin\phi_0 \\ \sin\phi_0 & \cos\phi_0 \end{bmatrix} \left(\begin{bmatrix} \cos\theta_0 & 0 \\ 0 & 1 \end{bmatrix} \begin{bmatrix} p_1 \\ p_2 \end{bmatrix} + \begin{bmatrix} \alpha_0(\sqrt{p_1^2+p_2^2})\sin\theta_0 \\ 0 \end{bmatrix} \right). \tag{6.4}$$

The integral $I_{A_\mathcal{G}}$ was integrated numerically. Again with an error tolerance of $\epsilon_{\mathrm{rel}} = 10^{-6}$

Chapter 7

Results and discussion

7.1 Energy conservation

The scattering problem discussed in this thesis allows for neither absorption nor transmittance of the incident wave. Thus, one would expect the energy of the scattered part of the wave to be equal to that of the incident part, $\mathcal{U} = 1$. This section will give results for which areas of parameter space yields energy conservation for modest angles of incidence under the Kirchhoff model, and discuss this requirement as a validity criterion for the MDRC.

The MDRC was integrated over all scattering directions in the upper heimsphere to assess for which areas in parameter space $\mathcal{U}$ is close to unity. Figure 7.1 shows the results for $\mathcal{U}$ versus δ/λ and a/λ for normal incidence and Gaussian and exponential correlation functions. At first glance, one can see from the results that the Gaussian correlation has a larger region of parameter space where $\mathcal{U} \approx 1$ than the exponential correlation function.

Figure 7.2 shows $\mathcal{U}$ versus δ/λ and a/λ for $\theta_0 = 20°$. The results looks quite similar to the normal incidence case. However, looking more closely one sees that in the $\theta_0 = 20°$ case, the line indicating $\mathcal{U} = 0.99$ is shifted a little bit, freeing up a larger region of parameter space falling into the category of having $\mathcal{U} > 0.99$. This is consistent with what was mentioned in section 2.5: increasing θ_0 increases the range of validity for the Kirchhoff approximation as long as one limits oneself to modest values, $\theta_0 < 30°$. This is because introducing a non-zero angle of incidence reduces the Rayleigh roughness parameter defined in Eq. (6.2). This parameter appears numerous times in the equations for the MDRC in the form of the factor $(\alpha_0(q_\parallel) + \alpha_0(k_\parallel))\delta$. Also, the coherent scattered light's contribution to $\mathcal{U}$, given by Eq. (6.1), which is the dominating contribution when δ/λ is low, is expressed solely in terms of the Rayleigh roughness parameter.

Comparing the solid line in Figure 7.1a with the criterion for the validity of the Kirchhoff approximation in section 2.5, one in fact finds that this criterion predicts the Kirchhoff approximation to be OK even in areas of parameter space where $\mathcal{U}$ is not approximately unity. This validity criterion by Shi et al[11]. is defined so that error of the averaged peak amplitude is less than 1dB. This validity criterion also comes with the requirement that one only looks at scattering angles that are not too high: $\theta_s < 70°$ when $\theta_0 = 0$. For angles approximately this value or higher, one knows that the Kirchhoff approximation will overshoot due to lacking to take into account shadowing effects. Because it neglects multiple scattering, there is nothing that stops the surface from scattering light into unphysical angles, i.e. $\theta_s > 90°$ under the Kirchhoff approximation. And it is this fact that allows for energy conservation to seemingly be broken under the Kirhhoff

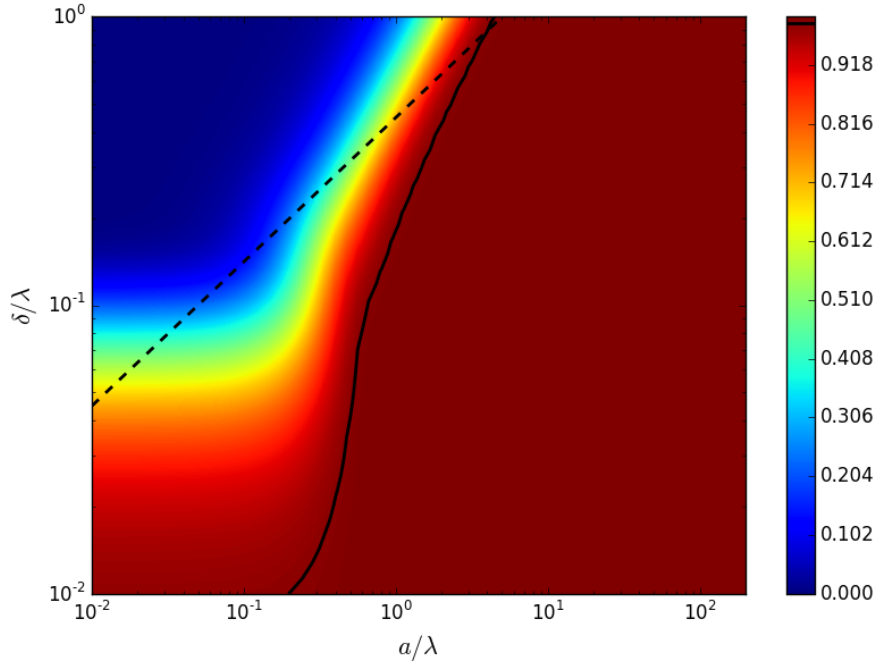

(a)

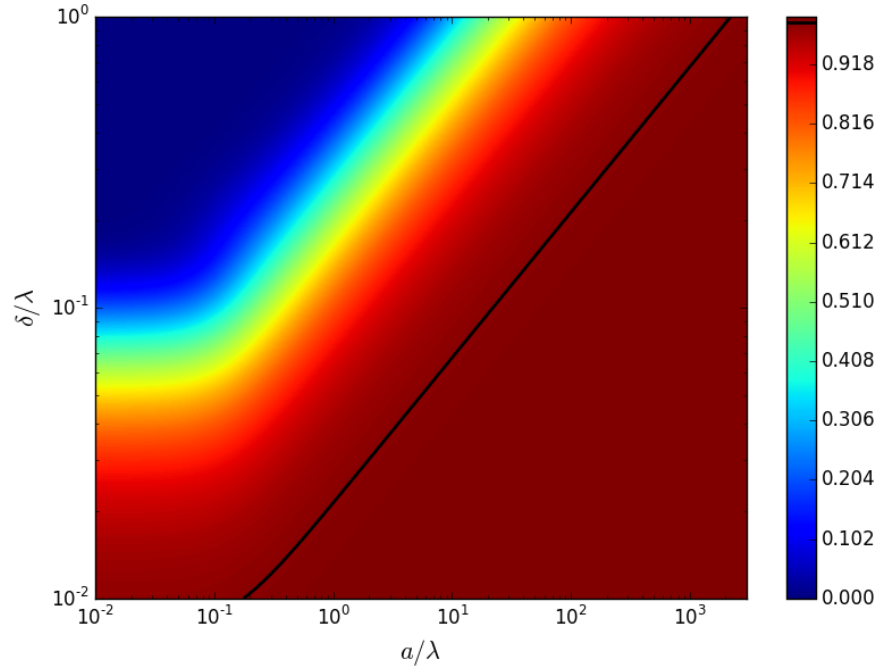

(b)

Figure 7.1: $\mathcal{U}$ vs. δ/λ and a/λ at normal incidence, $\theta_0 = 0$, for (a) Gaussian- and (b) exponential correlation functions. The solid line indicates where $\mathcal{U} = 0.99$. The dashed line indicates the validity criterion of Shi et al[11].

approximation.

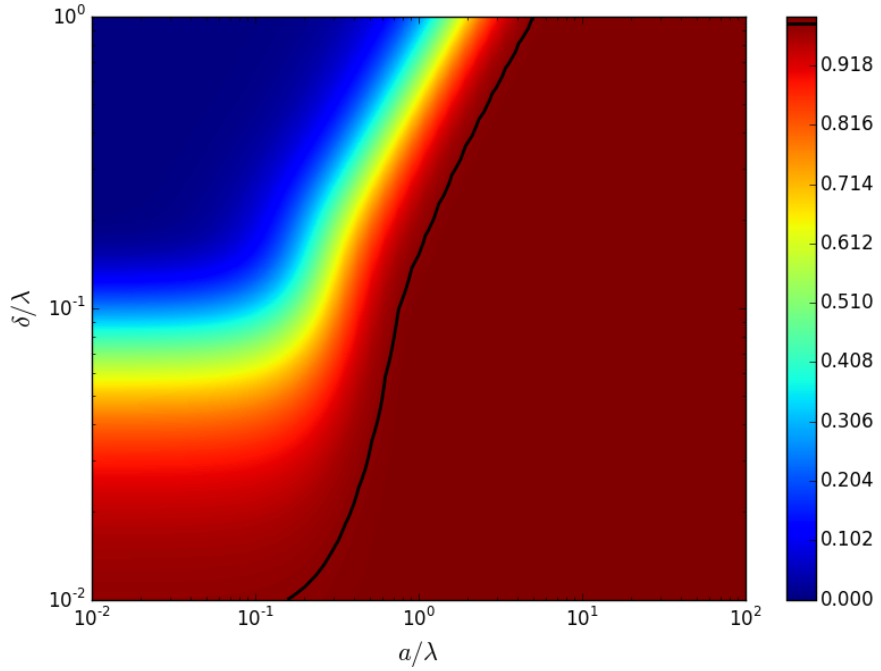

(a)

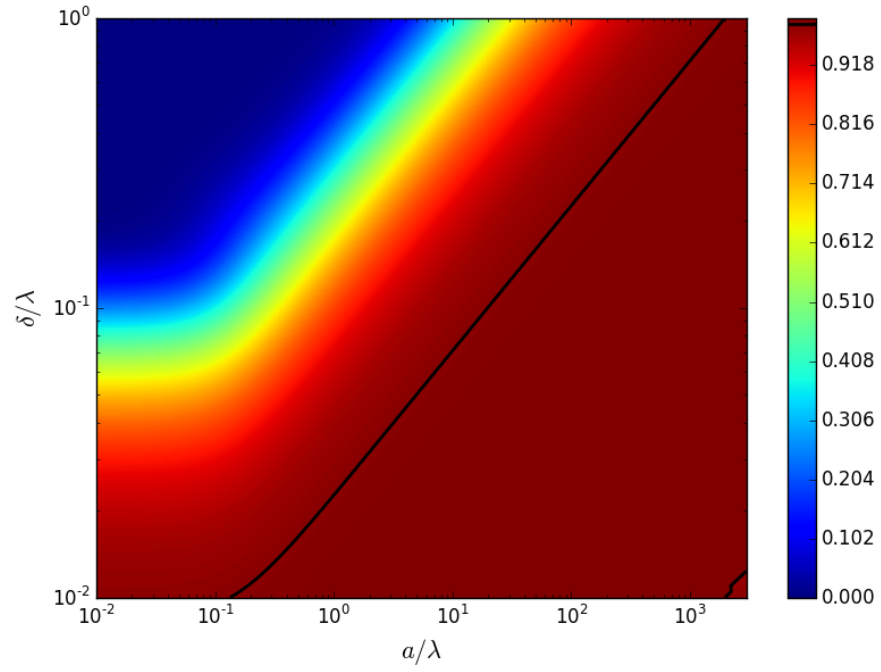

(b)

Figure 7.2: $\mathcal{U}$ vs. δ/λ and a/λ with $\theta_0 = 20°$, for (a) Gaussian- and (b) exponential correlation functions. The solid line indicates where $\mathcal{U} = 0.99$

7.2 Haze

Haze is plotted versus various parameters using both approximate analytical expression and integrating the MDRC numerically(Cubature). Unless mentioned otherwise, the number of terms used in obtaining the results for both cubature and approximation is set to some high

number making sure the sums have converged for all practical applications.

7.2.1 Contour plot

The haze was calculated over a wide range of parameters a/λ and δ/λ for the exponential and Gaussian correlation functions. Figure 7.3 gives a filled contour plot of the results when $\theta_0 = 0$. From the figure one can see that the Gaussian correlation function allows for studying a rather large area of parameter space with non-zero haze without violating energy conservation, here represented by the criterion $\mathcal{U} > 0.99$. For the exponential correlation function, this is not the case however. If one were to stick to the criterion $\mathcal{U} > 0.99$, only areas in parameter space where the haze is low, are left to be studied. The haze never gets above $H \approx 0.2 - 0.25$ within thea area with $\mathcal{U} > 0.99$. For the Gaussian correlation function we used two validity criterions, and it turned out that demanding energy conservation was a rather strict criterion. One can also study large areas of parameter space where this does not hold, as long as one does not look at too large values of the polar incident(θ_0) and/or scattering angles(θ_s). It might well be that the Kirchhoff approximation holds for modest angles in areas where the energy conservation is well beneath 0.99 also for the exponential correlation function, but not much is known about that at this point, and we are only left to speculate.

7.2.2 Versus correlation length

In Figure 7.4, haze is plotted versus correlation length on logarithmic scales for $\theta_0 = 20^\circ$ and $\Theta_{\text{lim}} = 2.5^\circ$. The red area shows where $\mathcal{U} < 0.99$ and again one can see that the Gaussian corrlation function has a larger area in parameter space where $\mathcal{U} \approx 1$, than the exponential correlation function. Furthermore, Figure 7.4 show that for high correlation lengths, the haze drops more rapidly for the Gaussian correlation function. The exponential correlation function drops of as a straight line in the logarithmic plot, implying that it goes as a power law, $\mathcal{H} \sim (a/\lambda)^c$, for higher correlation lengths, where c is a number determined by the inclination of the line.

In the areas with $\mathcal{U} > 0.99$ a good match is found between the approximation and cubature results for the Gaussian correlation function. The exponential correlation function also has a decent match, but the error is a bit higher. Moving into the low correlation length end of plots 7.4(a)-(d) where $\mathcal{U}$ is far from unity, one sees that the cubature and approximation results start to diverge. This comes from the assumption that $\mathcal{U} = 1$ in the approximate analytical expression. Calculating the haze as:

$$\mathcal{H} = 1 - \frac{1}{\mathcal{U}} \int_{\Delta\Omega_s} \left\langle \frac{\partial R}{\partial \Omega_s} \right\rangle \mathrm{d}\Omega_s, \tag{7.1}$$

for a given δ/λ, it is clear that as the correlation length gets shorter, the haze will increase due to the part of the integral in Eq. (7.1) representing the incoherent part of the MDRC getting smaller and smaller. The coherent part is however unchanged. As one moves to even shorter correlation lengths, $\mathcal{U}$ starts to drop for the cubature results, making the haze drop as well. One would not expect this kind of behaviour experimentally or for a rigorous simulation. Instead one would expect $\mathcal{U}$ to remain at unity and the haze to go to a constant value. This value is not necessarily the same as the one predicted by the approximate analytical expression, though. For very rough surfaces the MDRC is expected to become something like having the angular distribution of a Lambertian diffuser, having a $\propto \cos\theta_s$ dependence, independent of angle of incidence[13]. For such a surface one would expect the value of haze to become $\mathcal{H} \approx 1 - \sin(\Theta_{\text{lim}})$ for normal incidence, which amounts to $\mathcal{H} \approx 0.956$ for $\Theta_{\text{lim}} = 2.5^\circ$.

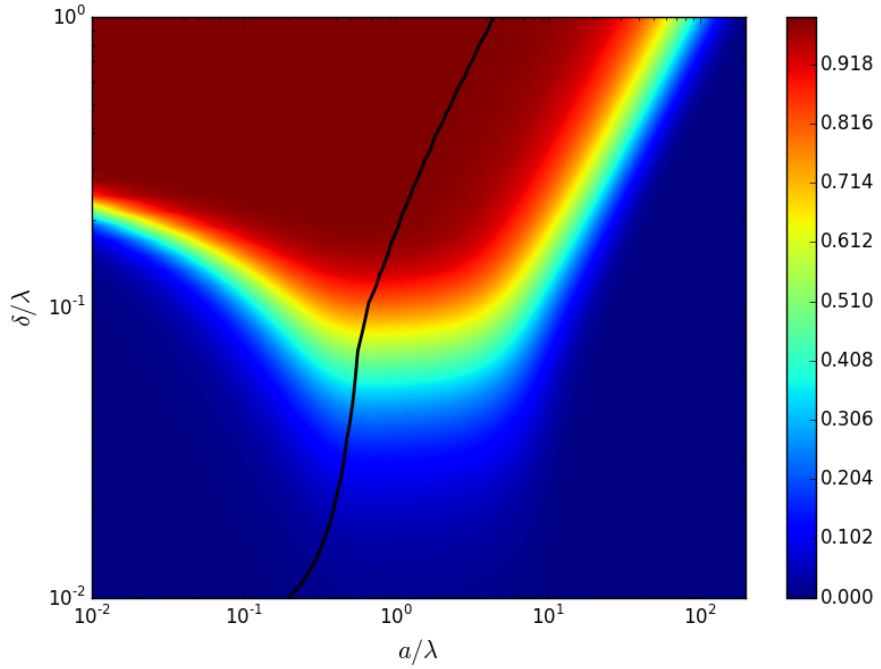

(a)

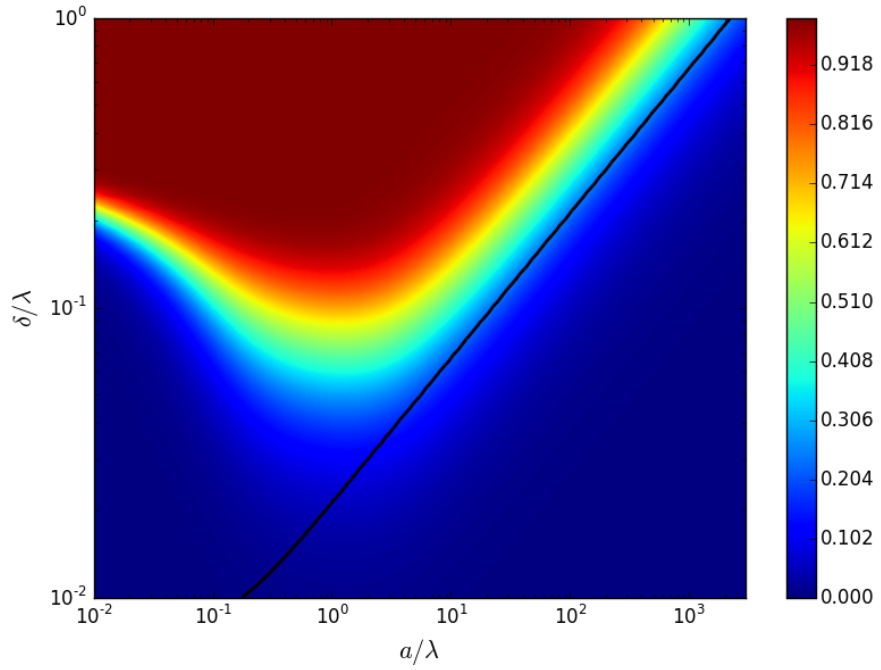

(b)

Figure 7.3: $\mathcal{H}$ vs. δ/λ and a/λ with $\Theta_{\text{lim}} = 2.5°$ at normal incidence and (a) Gaussian- and (b) exponential correlation functions. The solid line indicates where $\mathcal{U} = 0.99$.

7.2.3 Versus rms-roughness

In Figure 7.5 the haze is plotted versus δ/λ. The results for the Gaussian and exponential correlation functions look quite similar. The haze values for the Gaussian correlation function are however somewhat lower than those of the exponential. Once again, it is clear that the

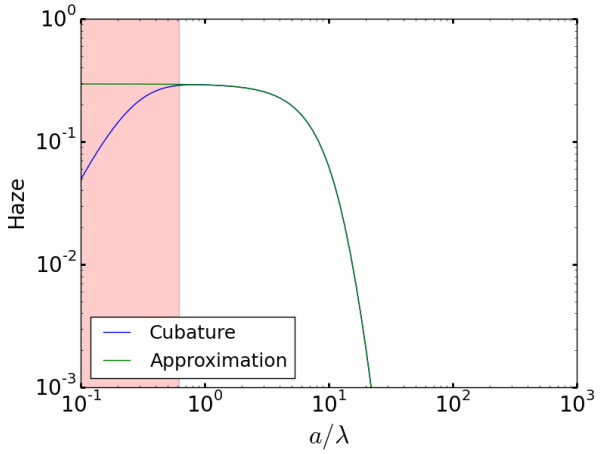

(a) $\delta/\lambda = 0.05$, $W(\boldsymbol{u}_\parallel)$ gaussian.

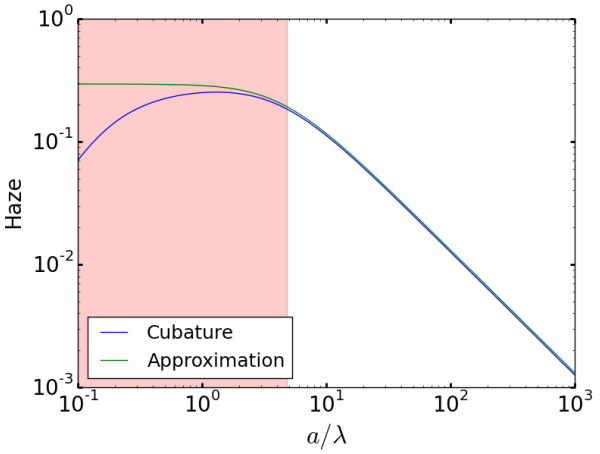

(b) $\delta/\lambda = 0.05$, $W(\boldsymbol{u}_\parallel)$ exponential.

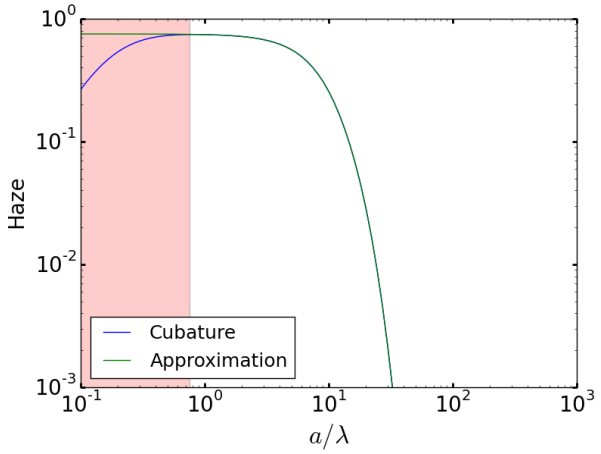

(c) $\delta/\lambda = 0.1$, $W(\boldsymbol{u}_\parallel)$ gaussian.

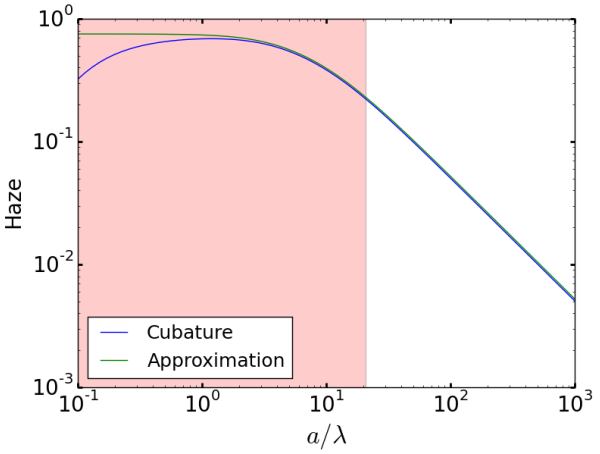

(d) $\delta/\lambda = 0.1$, $W(\boldsymbol{u}_\parallel)$ exponential.

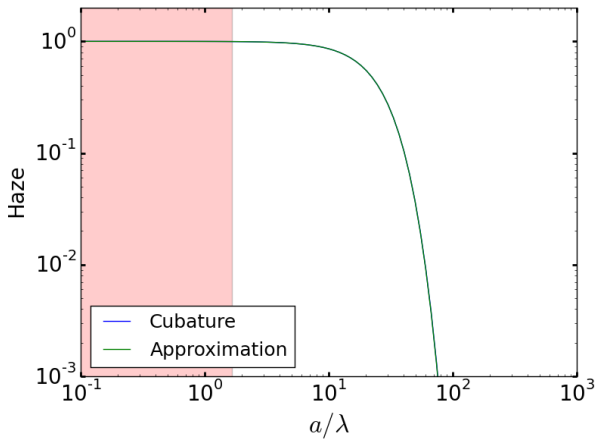

(e) $\delta/\lambda = 0.3$, $W(\boldsymbol{u}_\parallel)$ gaussian.

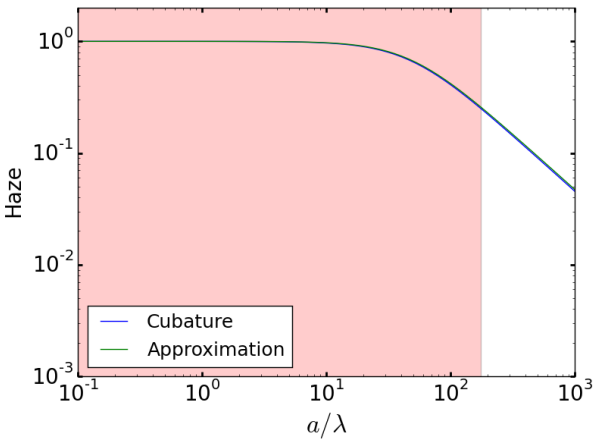

(f) $\delta/\lambda = 0.3$, $W(\boldsymbol{u}_\parallel)$ exponential.

Figure 7.4: Haze vs. a/λ for $\theta_0 = 20°$ and $\Theta_{\text{lim}} = 2.5°$. In the area shaded in red, $\mathcal{U} < 0.99$

Gaussian correlation function conserves the energy over larger regions of parameter space than the exponential.

In the limit where δ/λ is close to zero, the haze is dominated by the coherent contribution and

is approximately $\mathcal{H} \approx (1 - \exp[-(2R)^2])$, where R is the Rayleigh rougness parameter defined in (6.2). I.e. it is not dependent on the correlation function $W(\boldsymbol{u}_\parallel)$. The four subplots should therefore be identical when δ/λ is close to zero. As δ/λ increases, the incoherent part of the MDRC starts to contribute and the four plots start to show their differences. The plots then goes from being convex to concave and the haze starts to converge towards a constant close to 1.

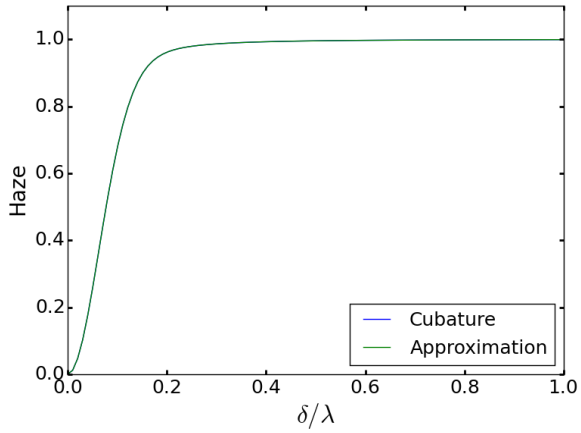

(a) $a/\lambda = 3.0$, $W(\boldsymbol{u}_\parallel)$ Gaussian.

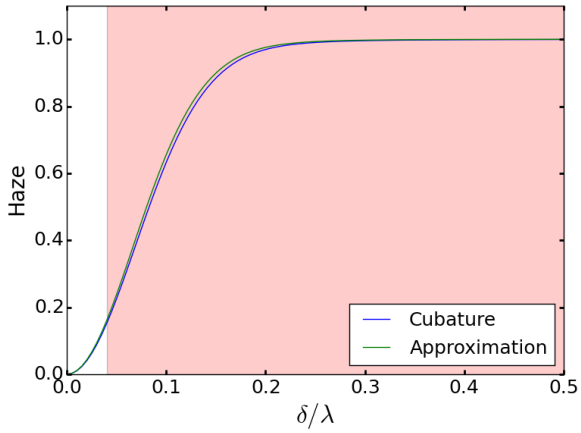

(b) $a/\lambda = 3.0$, $W(\boldsymbol{u}_\parallel)$ exponential

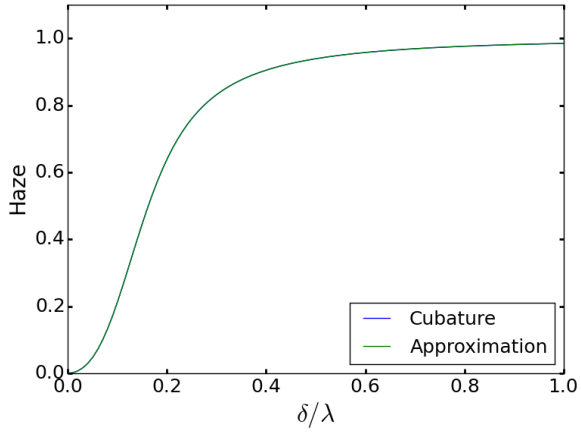

(c) $a/\lambda = 11.0$, $W(\boldsymbol{u}_\parallel)$ Gaussian.

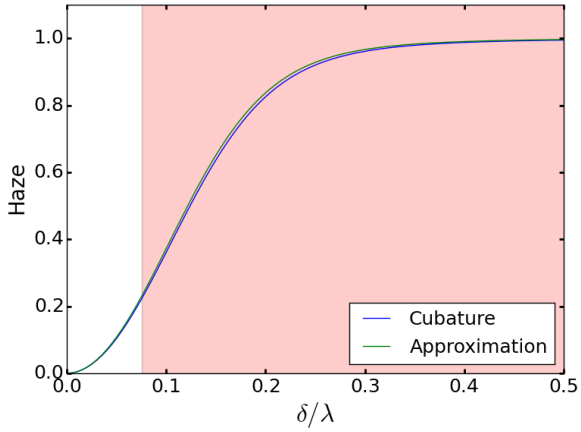

(d) $a/\lambda = 11.0$, $W(\boldsymbol{u}_\parallel)$ exponential.

Figure 7.5: Haze vs. a/λ for $\theta_0 = 20°$ and $\Theta_{\text{lim}} = 2.5°$. In the area shaded in red, $\mathcal{U} < 0.99$. Note the different x-axes for the two correlation functions.

7.2.4 Error in approximate expression

As has been shown, there is some error in the approximate expression for the exponential correlation function, while for the gaussian correlation function the error is smaller. The main reason that the approximate analytical expression for the exponential correlation function performs poorer than the Gaussian is, as will be shown, due to the first approximation of $\mathcal{U} \approx 1$. For the exponential correlation function, $\mathcal{U}$ simply never quite gets close enough to 1 in the interesting areas of parameter space.

Figure 7.6 plots the relative error versus a/λ between the approximation results and the cuba-

ture results twice. Once in the regular way, and once using $\mathcal{U}$ calculated by cubature in the approximate expression. For the exponential correlation function, the relative error, defined by $|\epsilon_r| = |\mathcal{H}_{\text{approx}} - \mathcal{H}_{\text{cubature}}|/|\mathcal{H}_{\text{cubature}}|$, shrinks by more than an order of magnitude over all the a/λ included in the analysis, when calculating $\mathcal{U}$ by cubature. Even when a/λ becomes as large as 1000, the graphs show no intention of converging for the exponential correlation function. The results for the Gaussian correlation function are also improved somewhat, but are already deemed acceptable. One can also see that the two graphs for the Gaussian correlation function having converged and being indistinguishable around $a/\lambda = 5$, indicating that $\mathcal{U} = 1$. The same parameters as in Figure 7.4(c)-(d) were used, giving us a reference point as to what the haze was.

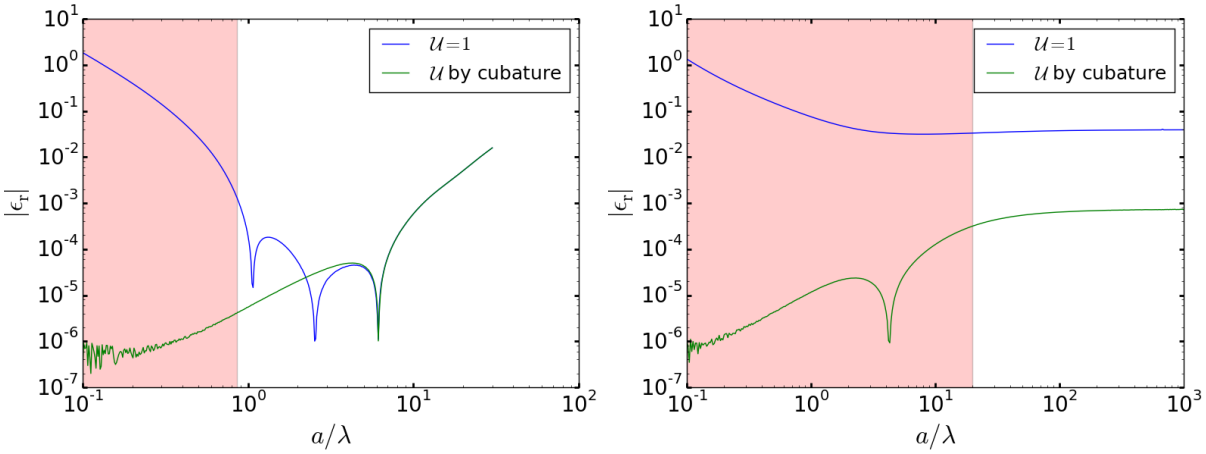

(a) $W(u_\parallel)$ Gaussian

(b) $W(u_\parallel)$ exponential

Figure 7.6: Error in the approximate expressions for haze. The blue line uses $\mathcal{U} = 1$ in the approximate expression as usual. The green line uses $\mathcal{U}$ calculated by cubature. $\theta_0 = 20°$, $\delta/\lambda = 0.1$, $\Theta_{\text{lim}} = 2.5°$.

7.2.5 Anisotropic effect

The haze from a surface described by a Gaussian anisotropic correlation function was calculated over a series of incident azimuth angles ϕ_0. The results are presented in Figure 7.7. The figure shows that the haze varies slightly with the azimuthal angle of incidence, ϕ_0, which one would excpect for an anisotropic surface. This effect is also described by the approximate expression for a general correlation function, given by the green line in Figure 7.7. In the special case where the anisotropic correlation function is Gaussian, not much computational effort is saved by using the approximation. The results does, however, give testament to the applicability of the approximation, given by Eq. (5.11).

If the approximation for a Gaussian aniostropic correlation function was used instead of the general correlation function approximation, one would not expect to describe the effect where the haze varies with ϕ_0. The reason for this is that in the former expression, the approximation is made that the integration of the MDRC is made over $\boldsymbol{Q}_\parallel$ and is approximated by a circular integration area. As stated earlier, this is only true for $\theta_0 = 0$. As θ_0 increases, part of this area is excluded due to the contraction of the minior axis of the elliptic integration area, $A_\mathcal{G}$. The aniostropic effect of haze being dependent of ϕ_0 comes from the fact that what parts of the MDRC is excluded form the integration area as θ_0 increases, is dependent on the orientation of

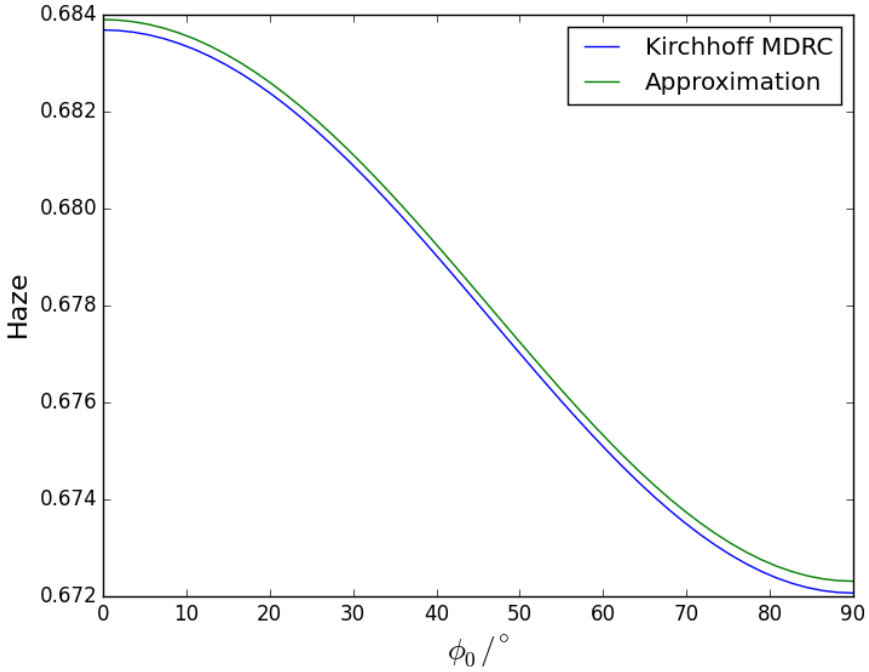

Figure 7.7: Haze vs. ϕ_0 for anisotropic correlation function. $\delta/\lambda = 0.2$, $a_1/\lambda = 7$, $a_2/\lambda = 14$, $\theta_0 = 30°$,$\Theta_{\text{lim}} = 2.5°$. The approximation used is the one for a general correlation function.

the elliptic area $A_{\mathcal{G}}$(and thus ϕ_0). For the same reason, one expects that the magnitude of the difference between haze at 0° and 90° increases with θ_0.

7.3 Dependence on wavelength and incident polar angle

In the previous section, various plots were made of the haze versus a/λ and δ/λ. In reality the surfaces must have specific values of a and δ, and so the haze will in general vary with the wavelength of the incident light. Figure (7.3) shows that there are multiple sets of parameters δ and a giving the same value of haze for a given angle of incidence, and thus it might be of interest to see how the different choices vary when it comes to the haze's dependence on θ_0 and λ. Having established the validity of the approximate expression for haze for Gaussian correlation functions, it is used to study the problem.

Say, one wanted a surface giving $\mathcal{H} = 0.65$ at normal incidence, with $\Theta_{\text{lim}} = 2.5°$ and that said surface is sufficiently approximated by the model. Figure 7.8(a) depicts the haze versus δ/λ and a/λ as calculated by the approximate expression for Gaussian correlation functions. All combinations of parameters δ and a, satisfying the validity criterion(dashed line) for the model, that lies on the solid line will, according to the model, yield the same haze of $\mathcal{H} = 0.65$. Figure 7.8(b) shows the derivative of the haze with respect to wavelength, $\frac{\partial \mathcal{H}}{\partial \lambda}$, along the solid line, parametrized in a/λ. The wavelength used was $\lambda_c = 600$ nm. $\frac{\partial \mathcal{H}}{\partial \lambda}$ starts out with a negative value of $\approx -1.2(\mu\text{m})^{-1}$ for small values of a/λ(and thus δ/λ), before steadily increasing and creeping towards zero as $a/\lambda \approx 30$ (and $\delta/\lambda \approx 0.5$). This indicates that the haze might be more stable when varying the wavelength for high-δ, high-a solutions in this particular case. This is confirmed by Figure 7.8(c), where the haze is plotted versus wavelength for two choices of parameters giving the same haze at $\lambda = \lambda_c = 600.0$nm. One with high values of both parameters,

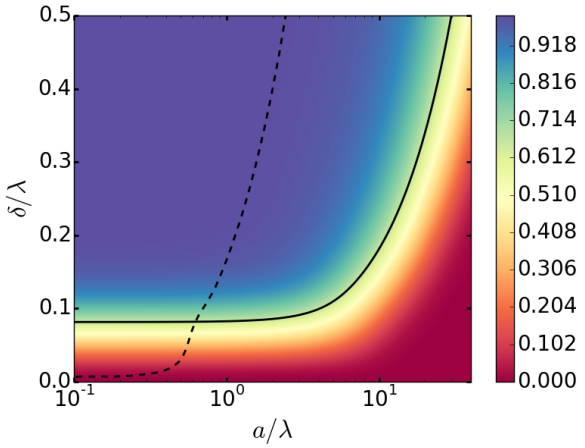

(a) Dashed line: $\mathcal{U} = 0.99$, solid line: $\mathcal{H} = 0.65$

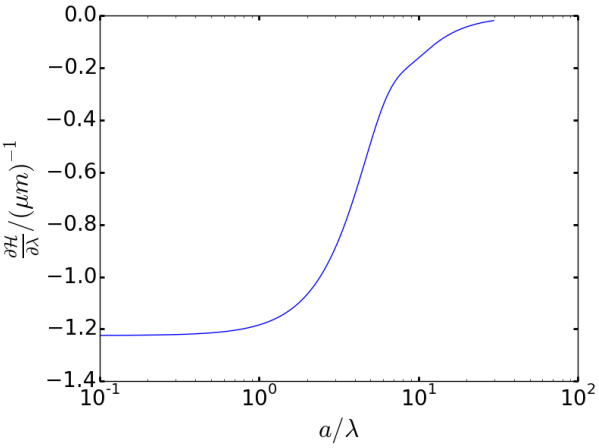

(b)

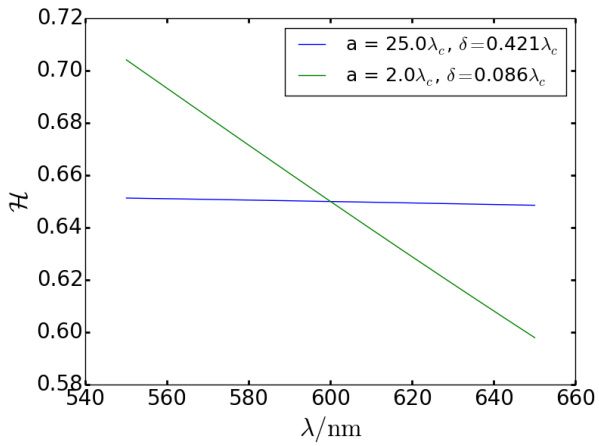

(c) $\lambda_c = 600.0$ nm

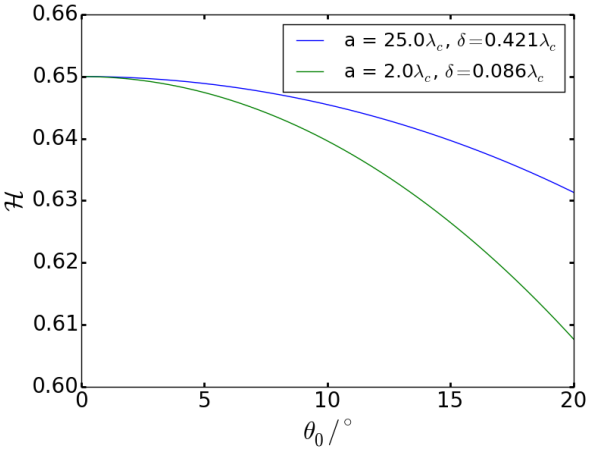

(d) $\lambda_c = 600.0$ nm

Figure 7.8: The haze versus a/λ and δ/λ in (a). The solid line indicates $\mathcal{H} = 0.65$ and the dashed line indicates $\mathcal{U} = 0.99$(validity criterion for the model). (b) shows $\frac{\partial \mathcal{H}}{\partial \lambda}$ along the solid line(parametrized in terms of a/λ). (c) and (d) shows how the haze varies with λ and θ_0 respectively for two choices of surface parameters on the $\mathcal{H} = 0.65$ line.

and one with low. Figure 7.8(d) shows how the haze varies with θ_0 for the same two sets of parameters. Having high values of δ and a is shown to also give a more stable haze when varying θ_0 in the given case.

$\frac{\partial \mathcal{H}}{\partial \lambda}$ being negative for low values of a/λ and δ/λ can be understood by assuming that the coherent part of the MDRC dominates in contributing to haze. Then $\mathcal{H} \approx 1 - \exp(-4\alpha_0^2(k_\parallel)\delta^2)$. The derivative can then be calculated analytically quite easily. Note, however, that it not always does continue to rise steadily like in the case given above. For certain choices of parameters, especially when looking for lower values of haze, the model will predict $\frac{\partial \mathcal{H}}{\partial \lambda}$ rising before reaching small positive values, and falling down again as one continues to move along the line with constant haze. For instance: at normal incidence, and with $\Theta_{\text{lim}} = 2.5^\circ$ and wavelength $\lambda_c = 600$nm, the two sets of parameters $(a = 2\lambda_c, \delta = 0.044\lambda_c)$ and $(a = 10\lambda_c, \delta = 0.096\lambda_c)$ are both predicted to give a haze of 0.25, but have different signs for $\frac{\partial \mathcal{H}}{\partial \lambda}$, with the latter having the positive value.

7.4 Comparison to rigorous scalar simulations

The results from the Kirchhoff model were compared to rigorous numerical simulations. The data used was the same as was used in the Master thesis of Torstein S. Hegge[7]. The simulations gives the MDRC of a scalar wave reflected off a hard gaussian correlated surface, averaged over approximately 3000 surface realizations. The rigorous simulations does, in contrast to the Kirchhoff model, take into account multiple scattering. However, some other differences between the two models must also be mentioned. The rigorous simulations uses surfaces with finite area and also uses incident beams that are superpositions of planewaves weighed by a Gaussian weight function to get beams of finite width. This fact will contribute to some additional differences between the results, especially when the roughness is low. Most prominently, the coherent part of the MDRC from the simulations is not a delta-function in the rigorous simulation, but rather a bell-curve shaped function, like the incident beam. In addition to this, the reader is reminded that, unlike the Kirchhoff model, the rigorous simulation's results are not invariant when changing the wavelength or surface boundary condition(neumann / dirichlet). For the rigorous simulations, the Dirichlet boundary condition and a wavelength of 1μm was used.

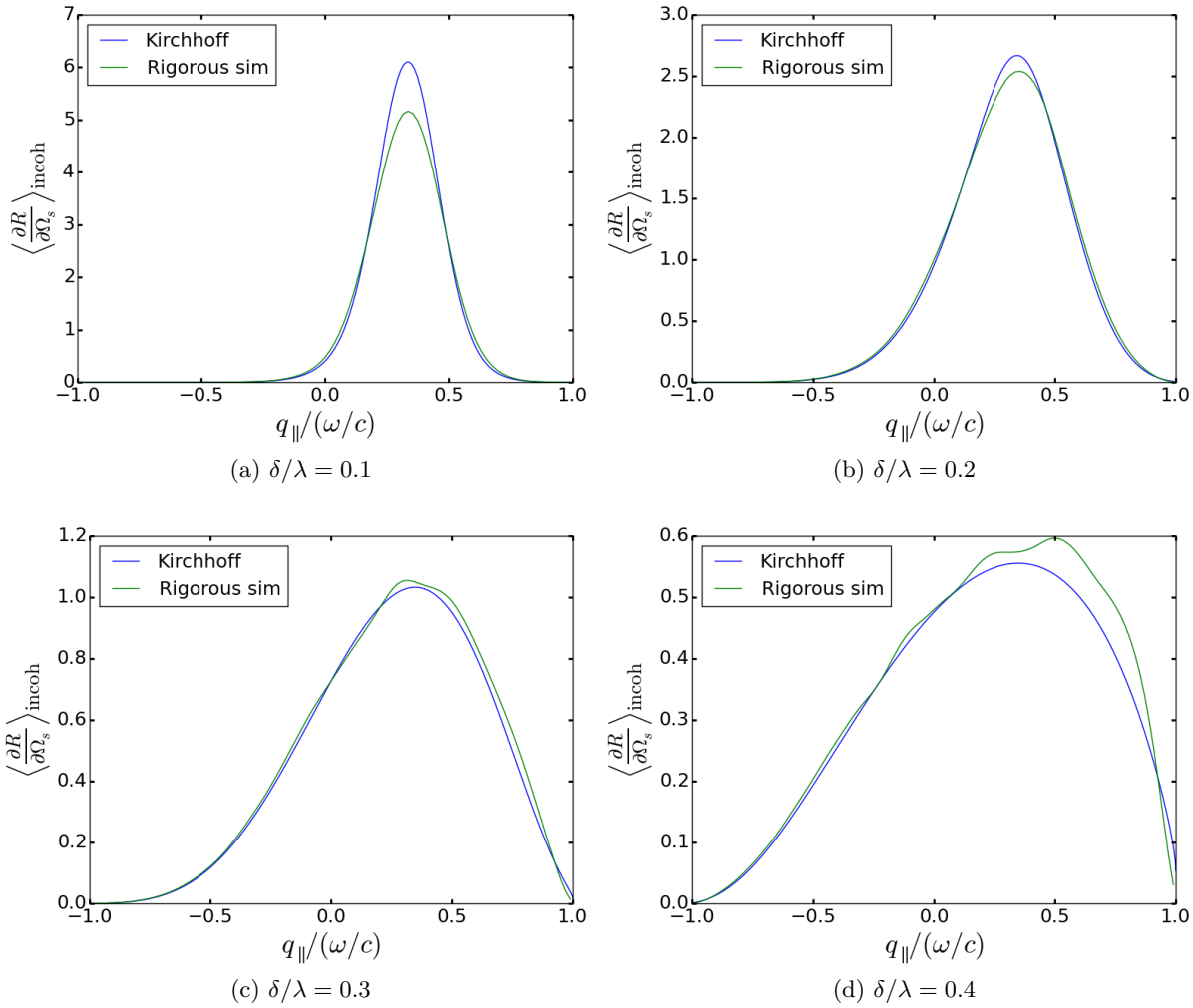

(a) $\delta/\lambda = 0.1$

(b) $\delta/\lambda = 0.2$

(c) $\delta/\lambda = 0.3$

(d) $\delta/\lambda = 0.4$

Figure 7.9: Incoherent part of the MDRC vs $q_\parallel$ along the plane of incidence. $a/\lambda = 2$, $\theta_0 = 20°$.

Figure 7.9 shows cuts of the incoherent part of the MDRC in the plane of incidence and compares it with the ones aquired from rigorous simulations. Bear in mind, however, that the results from

the rigorous simulations, due to a bug in the code, were found to have a total scattered energy fraction of $\mathcal{U} \approx 1.03$. We have been reassured that the bug only affected the normalization of the MDRC, and thus we expect the rigorous results for the MDRC to be a bit too high, but be fine otherwise. This effect is expected to disappear when discussing haze, since we always divide the integral over the MDRC by $\mathcal{U}$ when calculating haze. Going back to Figure 7.9 it is clear that there is a rather big disrepancy between the results when the rms roughness is low, and when the results would be expected to be the most alike. This is thought to be due to the fact that the coherent part of the MDRC are different for the two cases because of the different shape of the incident beams and the difference in area of the surface. A rather good match is found when $\delta/\lambda = 0.3$. Here, the coherent part of the MDRC has practically vanished, yet the roughness is apparently not too high for a decent match. When $\delta/\lambda = 0.4$, the differences between the rigorous simulations and the Kirchhoff model has become more pronounced.In Figure 7.9(c)-(d), where the MDRC is rather diffuse, the Kirchhoff approximation shows its tendency to overshoot for large scattering angles, due to neglecting multiple scattering, and thusly shadowing effects.

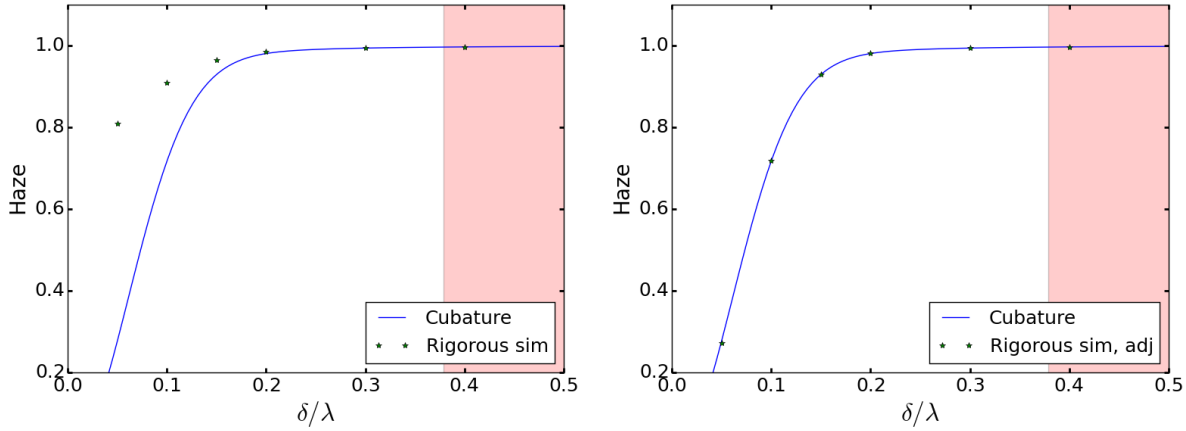

(a) $\Theta_{\text{lim}} = 2.5°$

(b) $\Theta_{\text{lim}} = 2.5°$

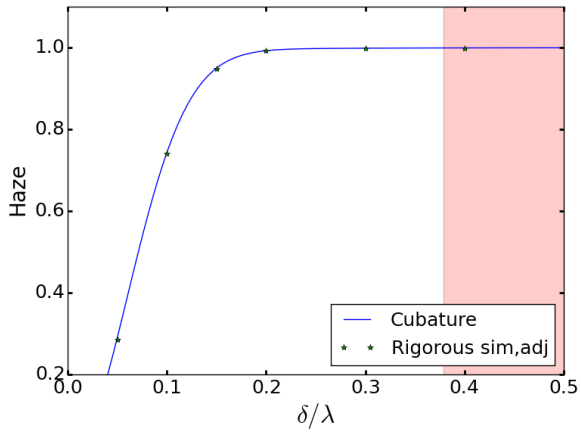

(c) $\Theta_{\text{lim}} = 1.25°$

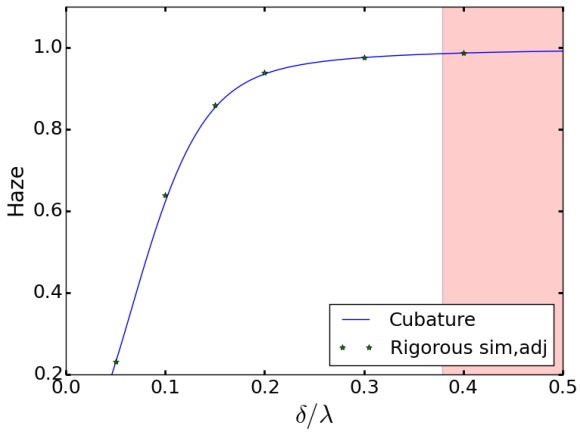

(d) $\Theta_{\text{lim}} = 5.0°$

Figure 7.10: Haze vs. δ/λ. Results from integrating the Kirchhoff MDRC are compared to data points made from integrating the MDRC from rigorous simulations. $a/\lambda = 2.0$, $\theta_0 = 20.0°$, $W(\boldsymbol{u}_{\parallel})$ Gaussian. $\mathcal{U} < 0.99$ in the red area.

Figure 7.10 shows the haze plotted against δ/λ for the Kirchhoff model, together with points

where haze has been calculated from the rigorous simulations. The MDRC was given on a 101x101 grid. For this reason a cubic spline interpolation was done before integrating the MDRC and calculating haze. For three of the subplots, the haze has been adjusted for the rigorous simulations. The total scattered energy for the coherent part of the MDRC for the rigorous simulations was calculated independently and simply assumed to contribute to gloss(I.e. the assumption that all of the coherently scattered energy went in the specular direction was made). Doing this adjustment, the figure shows that a decent match is found between the Kirchhoff model and the rigorous simulations when calculating haze. The rigorous scalar simulations was compared to simulations from an electromagnetic field scattered by a perfect conductor in Torstein S. Hegge's master thesis[7], where it was concluded that the results were comparable when the polarization of the scattered light was not recorded. Thus, this gives us hope that the Kirchhoff model at least could be applicable to approximating haze in this special case. Some further investigation will be made in the next section, where the Kirchhoff model is directly compared to two rigorous simulations of electromagnetic waves from a prefectly conducting Gaussian randomly rough surface.

7.5 Comparison to rigorous EM-simulations

The results of the model were compared to two rigorous simulations for the scattering of an electromagnetic wave from a perfectly conducting randomly rough surface. The EM-simulations are formally exact[14].The rigorous EM-simulations has, like the scalar simulations, a finite scattering area and a Gaussian incident beam. A Gaussian correlation function was assumed for the two simulations over incident angles $\theta_0 = 0^\circ$ and 20°, and the surface parameters were $\delta = 0.3\lambda$ and $a = 2\lambda$. The wavelength was 1μm. The rigorous simulations were averaged over 10000 surface realizations. Again the data was given on 101x101 grids, and was interpolated before studying haze. Figure 7.11 shows cuts of the MDRC for the two cases, in and out of the plane of incidence, for $\theta_0 = 20^\circ$. In addition it has a filled countour plot of the difference between the two MDRCs. For the EM-simulations, we look at the total intensity only, summing over outgoing polarizations and averaging over the incident polarizations, where the MDRC is given by $\frac{1}{2}(\mathrm{MDRC}_{pp} + \mathrm{MDRC}_{sp} + \mathrm{MDRC}_{ps} + \mathrm{MDRC}_{ss})$.

Figure 7.12 shows how the haze varies with Θ_{lim} for the rigorous simulations and Kirchhoff model. The relative error is also included. For the given simulation, the match seems to be good. The lines are almost indistinguishable, with the rigorous simulations having the slightly higher haze. This is consistent with the difference between the rigorous simulation MDRC and Kirchhoff MDRC around the specular direction in Figure 7.11. Around the specular direction, the figure shows that the MDRC for the Kirchhoff model is higher than that of the rigorous simulation, which will yield a lower haze.

All in all, the comparison with the electromagnetic simulations builds up under the the previous indications from the comparison to scalar simulations: The scalar Kirchhoff model seems to be a good approximation to the electromagnetic problem when the surface is assumed to be perfectly conducting and when the polarization of the scattered light is not recorded. One should bear in mind, however, that not only a small part of parameter space has been considered.

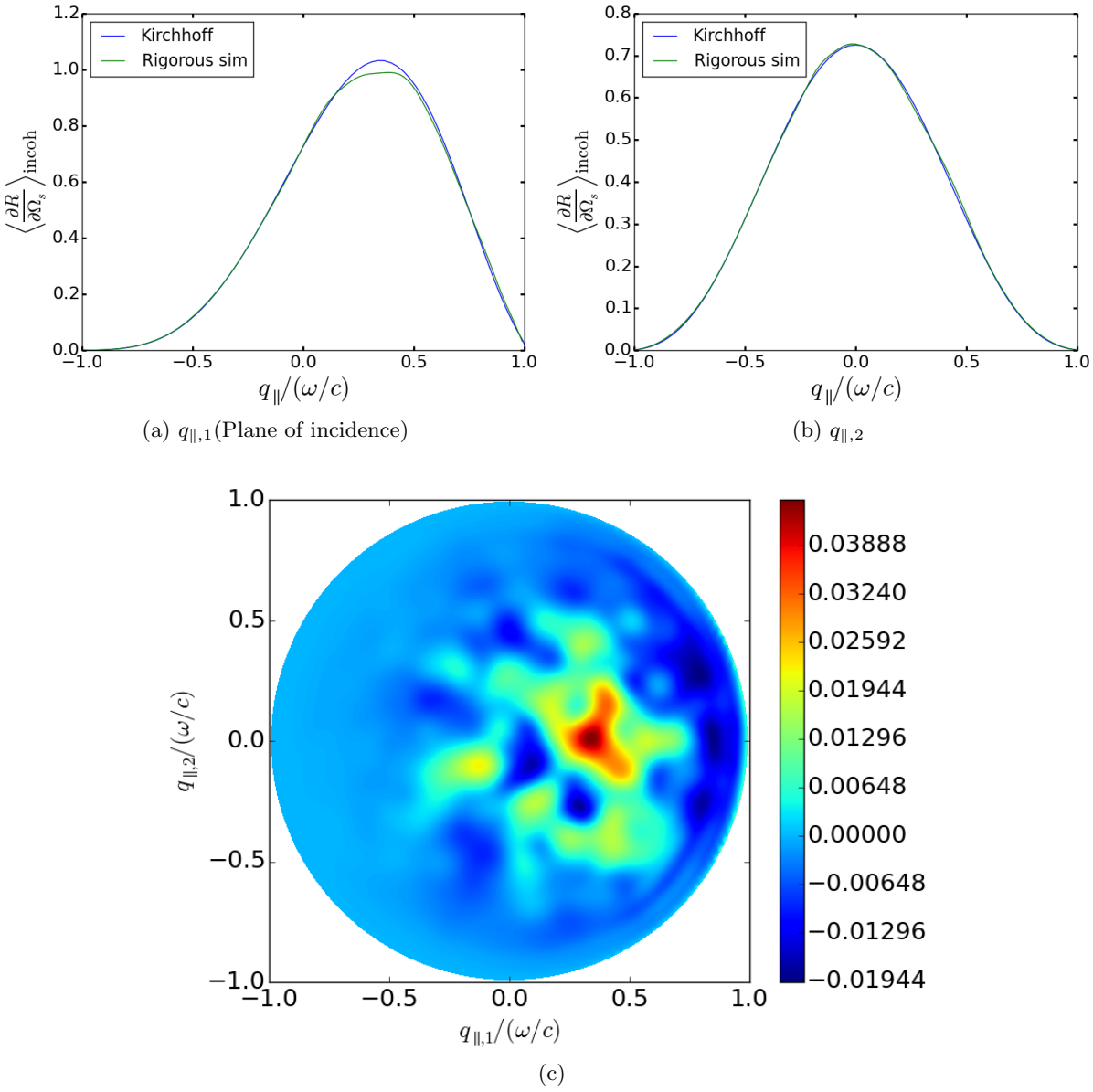

(a) $q_{\parallel,1}$(Plane of incidence)

(b) $q_{\parallel,2}$

(c)

Figure 7.11: MDRC for the rigorous EM-simulations and the scalar Kirchhoff approximation with (a) In-plane cut, (b) out-of-plane cut. Contour plot of the difference of the incoherent parts of the MDRCs in (c). Parameters used: $\theta_0 = 20°, \delta/\lambda = 0.3, \phi_0 = 0°$ and $a/\lambda = 2.0$.

7.6 Further work

Other surface models.

The model was earlier found to give comparable results to rigorous scalar scattering simulations that are known to be a good approximation to the scattering of EM waves by a perfect conductor when the polarization of the scattered beam is not recorded. However, one wants to be able to calculate haze from other surfaces as well, such as dielectrics or metals that does not conduct perfectly.

The tangent plane approximation of the scattering taking place from tangent planes at each

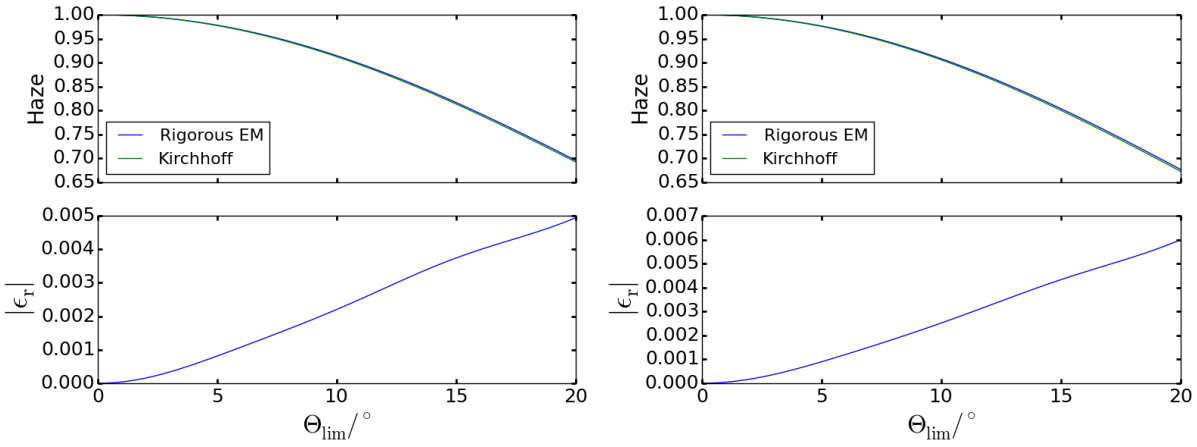

(a) $\theta_0 = 0^\circ$ (b) $\theta_0 = 20^\circ$

Figure 7.12: Haze vs. δ/λ. Results from integrating the Kirchhoff MDRC are compared to data points made from integrating the MDRC from rigorous simulations. $a/\lambda = 2.0$, $W(\boldsymbol{u}_{\parallel})$ Gaussian.

point of the surface, makes it natural to extend the model to dielectrics by applying the Fresnel equations locally. Such models have been studied before. For instance by Caron et al., who used a model based on the scalar Kirchhoff formalism to study scattering from dielectric randomly rough surfaces. The model gave good agreement with published data for reflection. For transmission there lacked published data.[5]

Validity of Kirchhoff approximation for arbitrary correlation functions

Before applying the model to exponential or other arbritrary correlation functions, more should be known about the validity of the Kirchhoff approximation for these correlation functions. The criterion $\mathcal{U} \approx 1$ could perhaps still be used as a guideline, but may be too strict in some cases.

Improvements on the current model

Improvements could be made upon the current model to make it perform better or stretch its limits of applicability without making the calculations more consuming.

The model could be improved without complicating the calculations considerably by introducing a shadowing function in the style of Beckmann to make the model more applicable for larger values of θ_0.[3]

Other corrections could also perhaps be made on the model on a purely empirical basis, when a greater understanding is aquired about the experimental results and rigorous simulations.

Inverse problem

An advantage of using a simple model such as the Kirchhoff model and the approximate expressions for haze based upon it, is that it has low computational cost. This gives an efficient base for

attacking the inverse problem of finding the rms-roughness and surface correlation that would give a surface having some pre-determined scattering properties related to haze. Methods such as photofabrication, gives the possibility of actually creating surfaces having a predetermined correlation function[4]. As stated earlier, not much is known in practice about the validity of the Kirchhoff approximation when the correlation function is no longer Gaussian.

Chapter 8

Conclusion

Haze in reflection was defined for scattering by two-dimensional surfaces, building on a method that previously often has been used for theoretical 1D studies of haze/gloss in a straight forward way. Under this definition, the gloss($\mathcal{G}$) and haze($\mathcal{H}$) are complimentary quantities related through the formula $\mathcal{G} + \mathcal{H} = 1$.

Haze was studied using a simple model, assuming a scalar wave, surfaces with Gaussian height-distributions and the Kirchhoff approximation. Haze was studied for the Gaussian and exponential correlation functions, including the conservation of energy for these surfaces under the model and how haze varies with the surface parameters a and δ. The haze's dependence on the azimuthal angle of incidence, ϕ_0, for an anisotropic Gaussian correlation functions was briefly studied.

Approximate analytical expressions for haze were derived for the isotropic gaussian and exponential correlation functions in the form of a sum. The expressions were found to match well with the results from manually integrating the Kirchhoff MDRC. Approximate expressions were also given for a general isotropic- and anisotropic correlation functions, this time in the form of a single and double integral, thus reducing the computational cost of calculating the haze for a general correlation function considerably.

The relationship between haze, λ and θ_0 was looked at, showing that different sets of surface parameters δ and a, all giving the same haze, gives surfaces that are predicted to having different properties when it comes to the haze varying with λ or θ_0. Specifically it was shown that for surface parameters giving $\mathcal{H} = 0.65$ at normal incidence with $\Theta_{\text{lim}} = 2.5°$ and $\lambda = 600.0$nm, choices with high-δ and high-a the haze changes less when varying λ and θ_0 than choices with low-δ and low-a for a Gaussian correlation function and when limiting the choices of rms-roughness to $\delta < 0.5$.

The model gave comparable results to simulations of EM-scattering from perfectly conducting surfaces, when using unpolarized incident light and when not recording the polarization of the scattered light. This was found by direct comparison to EM-simulations and also by comparison to scalar scattering simulations that are known to give comparable results to the EM-scattering problem.

Although its applicability is still limited to surfaces approximated by a perfect conductor, the model has given promising results. Both considering comparison to rigorous simulations and considering the simplicity of the approximate expressions for haze.

Bibliography

[1] SciPy. scientific computing tools for python. `http://www.scipy.org/`[Accessed 9. June 2015].

[2] Chapter 3 - Two-Dimensional Surfaces. In Alexei A. Maradudin, Eugenio R. Méndez, and Tamara A. Leskova, editors, *Designer Surfaces*, pages 201–305. Elsevier, Amsterdam, 2008.

[3] Petr Beckmann. Shadowing of random rough surfaces. *IEEE Transactions on Antennas and Propagation*, 13(3):384–388, May 1965.

[4] Vincent Brissonneau, Ludovic Escoubas, François Flory, and Gérard Berginc. Random rough surface photofabrication. volume 8172, pages 81720H–81720H–9, 2011.

[5] Jérôme Caron, Jacques Lafait, and Christine Andraud. Scalar Kirchhoff's model for light scattering from dielectric random rough surfaces. *Optics Communications*, 207(1–6):17–28, June 2002.

[6] I.S. Gradshteyn, I.M. Ryzhik, Victor Moll, and Daniel Zwillinger. *Table of integrals, series, and products*. Elsevier, Amsterdam, 2007.

[7] Torstein Storflor Hegge. Scalar wave scattering from two-dimensional, randomly rough surfaces. Master's thesis, NTNU, June 2011.

[8] Steven G. Johnson. Adaptive cubature. `http://ab-initio.mit.edu/wiki/index.php/Cubature`[Accessed 9. June 2015].

[9] Piotr Kowalczewski, Marco Liscidini, and Lucio Claudio Andreani. Light trapping in thin-film solar cells with randomly rough and hybrid textures. *Optics Express*, 21(S5):A808, September 2013.

[10] J. A. Ogilvy. *Theory of wave scattering from random rough surfaces*. Adam Hilger, Bristol, 1991.

[11] Fan Shi, Wonjae Choi, Elizabeth Skelton, Mike Lowe, and Richard Craster. Investigation of the validity of the elastic Kirchhoff approximation for rough cracks using a finite element approach. In *AIP Conference Proceedings*, volume 1650, pages 1722–1729. AIP Publishing, March 2015.

[12] I. Simonsen. Optics of surface disordered systems: A random walk through rough surface scattering phenomena. *The European Physical Journal Special Topics*, 181(1):1–103, January 2010.

[13] Ingve Simonsen, Åge Larsen, Erik Andreassen, Espen Ommundsen, and Katrin Nord-Varhaug. Haze of surface random systems: An approximate analytic approach. *Physical Review A*, 79(6):063813, June 2009.

[14] Ingve Simonsen, Alexei A. Maradudin, and Tamara A. Leskova. Scattering of electromagnetic waves from two-dimensional randomly rough perfectly conducting surfaces: The full angular intensity distribution. *Phys. Rev. A*, 81:013806, Jan 2010.

[15] Eric I. Thorsos. The validity of the Kirchhoff approximation for rough surface scattering using a Gaussian roughness spectrum. *The Journal of the Acoustical Society of America*, 83(1):78–92, January 1988.

Appendix A

Python code

Here follows some code in python, using the SciPy-stack[1]. It is also available digitally through the DAIM-system of NTNU.

MDRC

The following code gives a function that calculates the whole MDRC on a MxN grid in $q_1 q_2$, and utilizes it to plot the MDRC for a specific set of parameters:

```
import math
import numpy as np
import matplotlib.pyplot as plt

def alpha_0(x,wc):
    if wc*wc-x*x > 0:
        return np.sqrt(wc*wc-x*x)
    else:
        return 0

#Inputs:
#M: Number of points in y-direction
#N: Number of points in x-direction
#theta_0: Angle of incidence in radians
#a_r: Correlation length divided by lambda
#delta_r: Rms-roughness divided by lambda
#corr_func_choice: 'exp', 'gauss' or 'gauss_aniso'
#num_terms: Number of terms in the sum. High rms-rougness->many terms
#phi_0: azimuthal angle of incidence (Anisotropic corr.func. only)
#a_r_y: Corr.length / lambda in y-direction. (Anisotropic corr.func. only)
#
#Returns:
#qx - x component of lateral scattered momentum vector (array length N)
#qy - x component of lateral scattered momentum vector (array length M)
#mdrc - The incoherent part of the mdrc. (Grid MxN)
def mdrc_kirch(M,N,theta_0,a_r,delta_r,corr_func_choice,num_terms,phi_0=0.0,a_r_y
    =0.0):
    lamb = 1E-6         #Dummy wavelength.
    wc=2*math.pi/lamb #Length of momentum vectors: (w/c)

    a=a_r*lamb
    delt = delta_r*lamb
    ay=a_r_y*lamb
```

```
33
34      #Scattered lateral scattered momentum vector
35      qx_arr=np.linspace(-wc,wc,N)
36      qy_arr=np.linspace(-wc,wc,M)
37
38      #Incident lateral momentum vector and length
39      kv=wc*math.sin(theta_0)*np.array([math.cos(phi_0),math.sin(phi_0)])
40      klen=wc*np.sin(theta_0)
41
42      #Meshgrid of lateral scattered momentum vectors and length
43      qx,qy = np.meshgrid(qx_arr, qy_arr, sparse=False, indexing='xy')
44      qlen = np.sqrt(qx*qx+qy*qy)
45
46      #Make the if-else statement in alpha_0() work for arrays
47      valpha_0 = np.vectorize(alpha_0)
48
49      #Useful factor
50      alph2 = np.power(delt*(valpha_0(qlen,wc) + alpha_0(klen,wc)),2)
51
52      #Q_vec=q_vec-k_vec
53      Qx=qx-kv[0]
54      Qy=qy-kv[1]
55      Qx2=Qx*Qx
56      Qy2=Qy*Qy
57      Q2=Qx2+Qy2
58
59      #Do the sum
60      mdrc = np.zeros((M,N))
61      fac = np.ones((M,N))
62
63      #Case gaussian correlation function
64      if corr_func_choice == 'gauss':
65        for i in range(1,num_terms):
66            fac *= (alph2/i)
67            mdrc += fac*a*a*math.pi*np.exp(-0.25*Q2*a*a/i)/i
68
69      #Case gaussian anisotropic corr.func
70      elif corr_func_choice== 'gauss_aniso':
71        for i in range(1,num_terms):
72          fac *= (alph2/i)
73          mdrc += fac*a*ay*math.pi*np.exp(-0.25*(Qx2*a*a+Qy2*ay*ay)/i)/i
74
75      #Case exponential corr. func
76      elif corr_func_choice == 'exp':
77        for i in range(1,num_terms):
78          fac *= (alph2/i)
79          mdrc += fac*2*math.pi*a*a*i*np.power(float(i*i)+Q2*a*a,-1.5)
80      else:
81          print 'Error. Choose valid correlation function: exp, gauss or gauss_aniso
        '
82          return -1
83
84      #Multiply with prefactor
85      mdrc *= np.exp(-alph2)/(4*math.pi*math.pi*np.cos(theta_0))
86      mdrc *= np.power((wc*wc+valpha_0(qlen,wc)*alpha_0(klen,wc)-qx*kv[0]-qy*kv[1])
        ,2)
87      mdrc /= alph2/(delt*delt)
88
89      return qx_arr/wc,qy_arr/wc,mdrc
90
91  #Set parameters
92  M=201
```

```
N=401
theta_0=20.0*math.pi/180
phi_0 = 0.0*math.pi/180
delta_r = 0.3
a_r = 2.0
order = 200
corr_func = 'gauss'
a_r_y = 2.0

#Get the mdrc.
qx,qy,mdrc = mdrc_kirch(M,N,theta_0,a_r,delta_r,corr_func,order,0.0,0.0)

#Plot result
cs = plt.contourf(qx,qy,mdrc,500)
plt.colorbar(cs)
```

Approximate haze

The following code gives a function to calculate haze using the approximate expressions for Gaussian or exponential correlation functions, and applies it to calculate haze for several values of the correlation length.

```
import math
import numpy as np
import matplotlib.pyplot as plt

#Calculates haze by approximate expressions.
#
#Inputs:
#
#delt_r : rms-roughness divided by wavelength: delta/lambda
#a_r : corr. length divided by wavelength: a/lambda
#theta_0 : angle of incidence.
#Theta_lim : Limit angle. See 'definition of haze'.
#corr_func : 'exp' for exponential and 'gauss' for gaussian correlation func.
#num_terms : Number of terms in the sum.
#
#Returns: haze as number, array or grid, depending on inputs.
def haze_approx(delt_r,a_r,theta_0,Theta_lim,corr_func,num_terms):

    #Some factors that are useful
    alph_k = 2*math.pi*np.cos(theta_0)
    rf= 4*alph_k*alph_k*delt_r*delt_r

    #Radius of integration area in q_1q_2
    delta_q = 2*math.pi*np.sin(Theta_lim)*np.sqrt(np.cos(theta_0))
    df = a_r*a_r*delta_q*delta_q

    #Apply sum formula.
    tmp = 0
    fac = 1.0
    if corr_func == 'gauss':
        for i in range(1,approx_order):
            fac *= rf/i
            tmp += fac*(1-np.exp(-df/(4*i)))

    elif corr_func == 'exp':
       for i in range(1,approx_order):
            fac *= rf/i
```

```
            tmp += fac*(1-np.power(1+df/(i*i),-0.5))
    else:
        return 'no correlation function given'

    #Haze is 1 minus (coherent part + incoherent part) of gloss
    h_approx = 1.0-np.exp(-rf)*(1+tmp)

    return h_approx

#Set input values
delt_red = 0.3
theta_0 = 20.0*math.pi/180
Theta_lim = 2.5*math.pi/180
approx_order = 1000
corr_func = 'gauss'
cl_red=np.linspace(0.1,100,200) #Corr. length is an array in this example.

#Approximate haze
haze = haze_approx(delt_red,cl_red,theta_0,Theta_lim,corr_func,approx_order)

#Plot
plt.plot(cl_red,haze)
plt.xscale('log')
plt.yscale('log')
plt.ylim((1E-3,1))
```

Haze

In the thesis, haze was calculated in C using an adaptive integration routine on a function giving the incoherent part of the MDRC for a specific direction. Since this is expected to be slow in python, another approach will be given here(which also is not exactly fast): The MDRC is calculated on a MxN grid, interpolated and then integrated. This is not fool-proof and the user must inspect the MDRC to see if a finer grid is needed.

```
import math
import numpy as np
import scipy.integrate as integ
import scipy.interpolate as itp
from mdrc import mdrc_kirch #Import the function calculating mdrc on MxN grid

#Integrand when integrating over A_G
def integrand_g(Th,p,args):
    theta_0=args[0]
    phi_0=args[1]
    p1=p*math.cos(Th)
    p2=p*math.sin(Th)
    plen_sq = p*p
    alph=math.sqrt(1.0-plen_sq)
    qq1 = p1*math.cos(theta_0)+alph*math.sin(theta_0)
    qq2 = p2
    q1=qq1*math.cos(phi_0)-qq2*math.sin(phi_0)
    q2=qq1*math.sin(phi_0)+qq2*math.cos(phi_0)
    return p*f_mdrc(q1,q2)/alph

#Set parameters
M=600
N=500
theta_0=20.0*math.pi/180
```

```
phi_0 = 0.0*math.pi/180
Theta_lim = 2.5*math.pi/180
delta_r = 0.1
a_r = 5.0
order = 500
corr_func = 'gauss'
a_r_y = 2.0

#Arguments to pass to the integrand when integrating over A_G
argsi = []
argsi.append(theta_0)
argsi.append(phi_0)

#Get incoherent part of MDRC on MxN grid.
qx,qy,mdrc = mdrc_kirch(M,N,theta_0,a_r,delta_r,corr_func,order)

#Interpolate to get a function mdrc(qx,qy)
f_mdrc = itp.interp2d(qx,qy,mdrc,kind='cubic')

#Integrand when calculating U.
integrand_u_cart = lambda qx,qy: f_mdrc(qx,qy)/math.sqrt(1-qx*qx-qy*qy)

#Calculate integral over incoherent part of MDRC over all scattering angles.
    Cartesian.
a = integ.dblquad(integrand_u_cart, -1,1, lambda x: -math.sqrt(1-x*x), lambda x:
    math.sqrt(1-x*x),args=(), epsabs=1.49e-03, epsrel=1.49e-03)

#Calculate integral over incoherent part of MDRC over A_G. Polar coordinates.
b = integ.dblquad(integrand_g, 0,math.sin(Theta_lim), lambda x: 0, lambda x: 2*
    math.pi,args=(argsi,), epsabs=1.49e-08, epsrel=1.49e-08)

#Add coherent contributions.
u = a[0]+np.exp(-np.power(4*math.pi*delta_r*math.cos(theta_0),2))
g = b[0]+np.exp(-np.power(4*math.pi*delta_r*math.cos(theta_0),2))

#Print U
print u
#Print haze
print (1-g/u)
```

Approximate haze for a general correlation function

The following code calculates haze over azimuthal angles of incidence ranging from 0° to 90° for a general correlation function. In this case, the anisotropic Gaussian correlation function is used. It calculates the integral given in Eq. 5.11 in a polar coordinate system. I.e. $\mathrm{d}^2 v_{\parallel} \rightarrow |\boldsymbol{v}_{\parallel}|\mathrm{d}|\boldsymbol{v}_{\parallel}|\mathrm{d}\Theta_v$

```

import math
import matplotlib.pyplot as plt
import numpy as np
import scipy.special as sps
import scipy.integrate as integ

#Gaussian anisotropic corr. function
def W_gauss_aniso(ux,uy,args):
    ax=args[0]
    ay=args[1]
```

```
    return math.exp(-(ux/ax)*(ux/ax)-(uy/ay)*(uy/ay))

#Function that gives the upper integral limit of |v| as a function of Theta_v.
#Left for the reader to specify something more sophisticated.
def vmax(Th):
    return 15

#Evaluates the integrand for a given value of |v| and Th_v
def integrand(v,Th_v,args):
    alph2=args[0]
    d2=args[1]
    dp=args[2]
    costh0=args[3]
    s=args[4]
    c=args[5]
    W=args[6]
    W_args=args[7]

    vx=v*math.cos(Th_v) #Get cartesian x-value of integration variable
    vy=v*math.sin(Th_v) #Get cartesian y-value of integration variable
    ux=(vx*c/costh0 - s*vy)/dp #Get corresponding Delta x_1 value
    uy=(s*vx/costh0+c*vy)/dp    #Get corresponding Delta x_2 value

    y=(math.exp(4*alph2*d2*W(ux,uy,W_args))-1)*sps.j1(v) #Evaluate integrand
    return y



lamb = 457.9*1E-9
wc = 2*math.pi/lamb

##############################################################
#INPUT PARAMETERS

theta_0 = 30.0*math.pi/180
phi_0 = 0.0*math.pi/180
delta = 0.2*lamb
Theta_lim = 2.5*math.pi/180

#Choose correlation function
corr_func = W_gauss_aniso

#Arguments to be passed to the correlation function.
#Here: Correlation lengths for x- and y-direction, respectively.
corr_func_args=np.array([7*lamb,14*lamb])

#Error tolerance for scipy.integrate.dblquad()
abs_err = 1.0E-6
rel_err = 1.0E-6
##############################################################
argsi=[]
argsi.append(math.pow(wc*math.cos(theta_0),2))
argsi.append(math.pow(delta,2))
argsi.append(wc*math.sin(Theta_lim))
argsi.append(math.cos(theta_0))
argsi.append(math.sin(phi_0))
argsi.append(math.cos(phi_0))
argsi.append(corr_func)
argsi.append(corr_func_args)


N=50
```

```
74 phi_arr=np.linspace(0,math.pi/2,N)
75 haze_arr=np.zeros(N)
76
77
78 for i in range(0,N):
79     argsi[4]=math.sin(phi_arr[i])
80     argsi[5]=math.cos(phi_arr[i])
81     a = integ.dblquad(integrand,0,2*math.pi, lambda x: 0, vmax,args=(argsi,),
       epsabs=abs_err, epsrel=rel_err)
82     haze_arr[i] = 1-math.exp(-4*argsi[0]*argsi[1])*(1+a[0]/(2*math.pi))
83
84 plt.plot(phi_arr*180/math.pi,haze_arr)
```